

# **Carbonization of SU-8 Based Electrode for MEMS Supercapacitors**



**By Yang Liu**

This work has been carried out at Department of Micro and Nano Systems  
Technology, Buskerud and Vestfold University College, Norway  
under the supervision of

Professor Xuyuan Chen.

*Horten, May, 2014*

Submitted to the Faculty of Technology and Maritime Science, Buskerud and Vestfold University  
College, in partial fulfillment of the requirements for the degree Master of Microsystem  
Technology

## **Table of Contents**

<b>Abstract</b> .....	1
<b>Chapter 1 Introduction</b> .....	2
1.1 Background.....	2
1.2 The principle and classification of supercapacitors.....	4
1.3 History of supercapacitors technology.....	5
1.4 MEMS supercapacitors.....	7
1.5 State-of-art of MEMS supercapacitors.....	8
1.6 The topic of this thesis.....	10
<b>Chapter 2 Experiments</b> .....	12
2.1 System setup for lithography.....	12
2.2 System setup for carbonization.....	15
2.3 RIE technology.....	16
2.4 Wet etching technology.....	18
<b>Chapter 3 Micro Mechanical Interlocking</b> .....	20
3.1 Analysis of Micromechanical interlocking as the root.....	20
3.2 Fabrication process design for inverted-trapezoid pit.....	23
<b>Chapter 4 Fabrication Process of Inverted-trapezoid Pit</b> .....	26
4.1 Photolithography process.....	26
4.2 Anisotropic RIE etching process.....	28
4.2.1 Factors of RIE etching process.....	29
4.2.2 Experimental procedures and results.....	31
4.3 Anisotropic wet etching Si.....	33
<b>Chapter 5 Carbonization of SU-8 based Electrodes</b> .....	36
5.1 MEMS Supercapacitors based on SU-8 technology.....	36
5.1.1 SU-8 photoresist.....	36
5.1.2 Fabrication of SU-8 microstructure.....	38
5.2 Carbonization process.....	41
5.2.1 Carbonization process design.....	42

## **Carbonization of SU-8 based electrode for MEMS supercapacitors**

---

5.2.2 Temperature segment setting.....	43
<b>Chapter 6 Characterization of Carbonization Process and Carbon Films.....</b>	<b>47</b>
6.1 Film adhesion analysis.....	47
6.1.1 Thick film structure analysis.....	47
6.1.2 Thin film structure analysis.....	51
6.1.3 Summary.....	54
6.2 Weight loss analysis.....	55
6.3 Microscopy analysis.....	57
6.3.1 SEM images.....	57
6.3.2 Vertical shrinkage.....	58
<b>Chapter 7 Conclusion.....</b>	<b>60</b>
<b>Reference.....</b>	<b>61</b>
<b>Acknowledgement.....</b>	<b>64</b>

## **Abstract**

Supercapacitors are more sustainable and environmentally friendly energy sources than traditional ones. To achieve the supercapacitors with both energy density and power density that mainly depend on the effective surface area of the electrodes, SU-8 can be used for electrode material to fabricate 3D microstructures as the electrodes that increase the effective surface area significantly. The objective of this project is to fabricate the reliable electrodes of large surface area for supercapacitors by SU-8 process, in which the SU-8 films are carbonized in an inert atmosphere in high temperature furnace.

To improve the adhesion between the developed electrodes and the substrate is the key task in my thesis work. The micromechanical interlocking is proposed and designed for improving the adhesion which can also be optimized by controlling the heating and cooling rate in carbonization process. According to the force analysis, the inverted-trapezoid pits are the most reliable structures in the substrate as the root for SU-8 films. Inverted-trapezoid pits are obtained by combining both dry etching and wet etching technologies. The dry etching is very important to influence the depth of inverted-trapezoid structures.

Based on the characteristics of pyrolysis process for SU-8, in our experiments the highest carbonization temperature is chosen at such as 700°C, 900°C or 1000°C, respectively. We have found that after finishing the carbonization process, the carbon film is locked firmly on the substrate by the inverted-trapezoid pits, but the warping phenomenon appears in the thick films and cracks occur in the thin films. These problems can be solved by modifying the process parameters in fabricating the inverted-trapezoid pits and the SU-8 structure films. In addition, the weight loss and vertical shrink increase with increasing the carbonization temperature during this process.

# Chapter 1 Introduction

## 1.1 Background

Energy production from the combustion of fossil fuels is forecast to have a severe impact on world economics and ecology in the future. Electrochemical energy production is investigated as an alternative energy/power source, as long as this more sustainable and more environmentally friendly energy consumption is designed. The systems that is used for electrochemical energy storage and conversion include batteries, fuel cells, and supercapacitors. For energy storage devices, energy density and power density are very important parameters for characterizing the performance of the devices. Energy density defines the amount of energy that can be stored in a given volume or weight of the material. Power density defines the total energy per unit time which can be stored into the device. So the ideal storage device should have both of high energy density and high power density. To compare the power and energy capabilities, a representation known as the Ragone plot or diagram has been developed, it is shown in figure 1.1.<sup>[1]</sup> Batteries have high energy density, but poor power density. Fuel cells have the highest energy density, and lowest power density. By contrast with them, supercapacitors could possess high power density and notable increased high energy density.

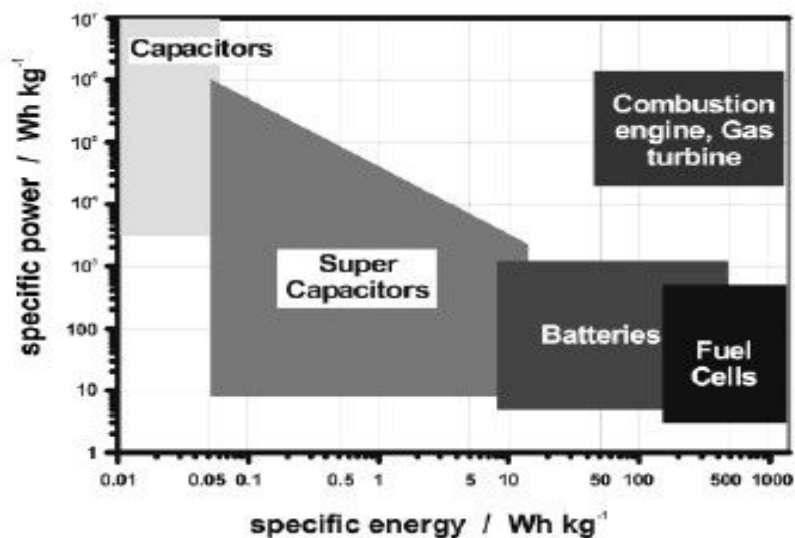


Fig. 1.1 Ragone plot of various energy storage devices<sup>[1]</sup>

## Carbonization of SU-8 based electrode for MEMS supercapacitors

Supercapacitors can provide much shorter charging and discharging time, low equivalent series resistance, virtually unlimited cycle life, and high operating temperature. So supercapacitors fill the gap between batteries and conventional capacitors. Table 1 shows the comparison of supercapacitors and batteries.<sup>[2]</sup>

The application prospect of supercapacitors is broad. The first application is electronic circuits or small electrical appliances. Typically, supercapacitor as a back-up power for storage device, such as in Japan's Niigata Prefecture,<sup>[3]</sup> has the first street lights that combine a stand-alone power source with solar cells and energy saving LED. Supercapacitors store the solar generated energy and supply two LED lamps, providing 15 W power consumption overnight. The supercapacitors ensures long life (>10 years) and stable characteristics under various climates, allowing the lights to operate in a wide range of temperatures, from over 40°C in summer to below -20°C in winter. The second application is combined with the battery provide high power. For example, as a hybrid electric vehicle auxiliary power, a bus powered by supercapacitors is developed by Taiwan research group in 2006, that was used for stop and go application,<sup>[4]</sup> the bus charged at an inductive power transfer station for about 3 minutes, the energy of 1.5KWh is transferred to the supercapacitors on the bus for a ride of 3Km.

Table 1. comparison of supercapacitors and batteries<sup>[2]</sup>

Device	Charging time	Discharging time	Cycle life	Specific power(W/kg)	Specific energy(Wh/kg)
Capacitors	μsec-msec	μsec-msec	10 <sup>6</sup> -10 <sup>8</sup>	>10000	<0.01
Super capacitors	msec-minute	msec-minute	10 <sup>6</sup> -10 <sup>8</sup>	1000-3000	0.5-5
Battery	hours	minutes-months	200-1000	<500	50-300

## 1.2 The principle and classification of supercapacitors

Supercapacitors can be classified into electric double layer capacitor (EDLC), electrochemical pseudo capacitor (EPC) and hybrid capacitor by charge storage mechanisms.

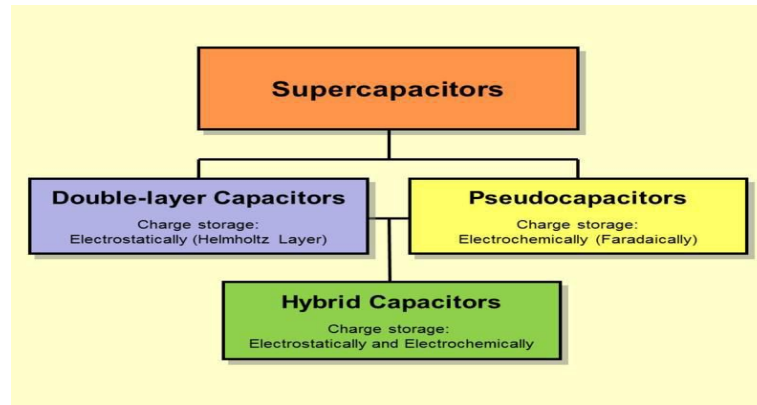


Fig. 1.2 Classification of supercapacitors<sup>[5]</sup>

For different supercapacitors, they have different electrode materials. Carbon materials<sup>[6-7]</sup> in different forms such as carbon fibers, carbon aerogels, activated carbons and carbon nanotubes are most commonly used high specific area electrode materials for double layer capacitor. These materials exhibit various attractive physical and chemical properties such as high conductivity, high surface area, high temperature stability, good corrosion resistance, high porosity, easy processability and good compatibility in composite materials and relatively low cost.

The electrode materials of pseudo capacitor is transition metal oxides and conducting polymers. Metal oxides<sup>[8]</sup> such as  $\text{RuO}_2$ ,  $\text{NiO}$ ,  $\text{Co}_3\text{O}_4$ ,  $\text{MnO}_2$  etc. They have been widely investigated for electrode materials of ES, because they have high specific capacitance at low resistance. Conducting polymers such as Polypyrrole (PPY), Polyaniline (PAn) and Polythiophene (PTh) are considered as the promising electrode materials.

The storage principle of double layer capacitor is shown in Fig. 1.3.<sup>[9]</sup> By applying a voltage to the capacitor at both electrodes, a respective Helmholtz double layer is

## Carbonization of SU-8 based electrode for MEMS supercapacitors

formed, which has a positive or negative layer of ions from the electrolyte deposited in a mirror image on the respective opposite electrode.

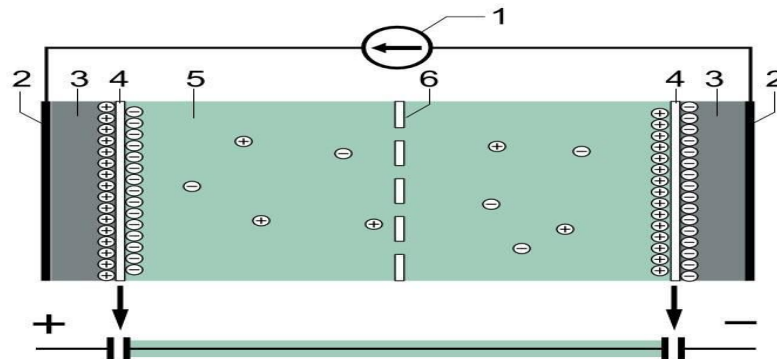


Fig. 1.3 Working principles of EDLC

1. power source, 2. Collector, 3. polarized electrode, 4. Helmholtz double layer
5. electrolyte having positive and negative ions, 6. Separator

Pseudo capacitor has fast reversible redox reactions occurring at the surface of electrode. Fig. 1.4 shows the working principles of pseudo capacitor.<sup>[10]</sup>

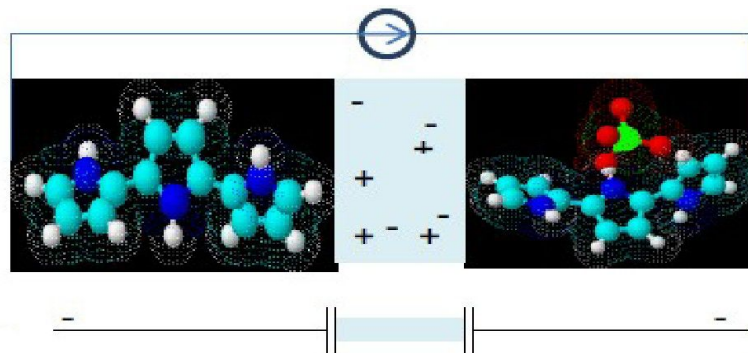


Fig. 1.4 Working principle of EPC

### 1.3 History of supercapacitors technology

The electric double-layer capacitor was first noticed in 1957 by General Electric engineers experimenting with devices using porous carbon electrode.<sup>[11]</sup> Eventually Standard Oil of Ohio's (SOHIO)<sup>[12]</sup> researchers developed the modern versions of devices and achieved higher energy density by utilizing the double-layer capacitance of high area carbon in a non-aqueous electrolyte, in 1966.

## Carbonization of SU-8 based electrode for MEMS supercapacitors

In 1978, the term “supercapacitors” was quoted by NEC under the licenses of SOHIO, to supply backup power for maintaining computer memory.<sup>[13]</sup> Also in the same year Panasonic began manufacturing double-layer capacitors, called “Gold cap”, in Japan. These were initially developed primarily to replace the unreliable cell batteries used in memory back-up applications at that time. The major differences between the Panasonic and NEC products were the electrolytes; NEC used an aqueous electrolyte in a “pasted electrode” with bipolar cell construction; Panasonic, on the other hand, used a non-aqueous electrolyte and pasted electrode in the cell construction. The advantages of the Panasonic electrolyte is a higher unit cell operating voltage.

Between 1975 and 1981 a different principle capacitors that called pseudo capacitors, was developed by B. Conway.<sup>[14]</sup> Ruthenium oxide was the first expanded material to prepare the electrodes of pseudo capacitors. However, the Ru-based materials are very expensive. Therefore, researchers investigated other metal oxides, such as manganese oxides and others. In 2005, aerospace systems and controls company choose ultracapacitors Boost cap (Maxwell Technologies) to power emergency actuation systems for doors and evacuation slides in passenger aircraft, including the new Airbus 380 jumbo jet. Fig. 1.5 shows the Boost cap of Maxwell.<sup>[15]</sup> In 2006, Joel Schindall and his team at MIT began working on a "super battery", using nanotube technology to improve upon capacitors.



Fig. 1.5 A Maxwell Boost cap<sup>[15]</sup>

## **Carbonization of SU-8 based electrode for MEMS supercapacitors**

Recently, all solid state micrometer-scale electric double-layer capacitors that based on advanced super ionic conductors have been used for low voltage electronics in future, such as deep-sub-voltage nanoelectronics and related technologies. The market for EDLC is currently valued at approximately a half-billion dollars and continues to grow. Today several companies such as Maxwell Technologies, NEC/TOKIN, ELNA, Panasonic, and several others invest in electrochemical capacitor development.<sup>[16]</sup>

### ***1.4 MEMS supercapacitors***

MEMS supercapacitors mean Micro Electrical Mechanic System supercapacitors. MEMS supercapacitor is basically a miniaturized supercapacitor in micro scale or nano scale. Usually, supercapacitors are widely applied as backup power sources for memories, microcomputers, system boards, and clocks. Commercially available products are difficultly integrated in many compact applications because of their big size. Especially, miniaturizations of systems require compact capacitors of high specific capacitance and miniaturized power sources of high energy and power density. Integration of supercapacitors within systems on chip or in circuits is a developing target. Hence, miniaturization of supercapacitors by MEMS technology is required.

For fabricating a MEMS supercapacitor, We focus on the specific surface area of electrodes. Because the larger surface area leads to larger capacitance, the capacitance is a sign that the energy is stored by the supercapacitor. The basic challenge is how to increase the surface area for a compact supercapacitor by innovation design and fabrication technology. Using MEMS technology to fabricate a high aspect ratio (HAR) 3D electrode is an efficient way. Because it is able to greatly create more surfaces in a given footprint. In recent years, SU-8 has become new approach for making electrodes of supercapacitors.<sup>[17-20]</sup> SU-8 is a negative photoresist which suitable for high aspect ratio structures.

As an example, Fig. 1.6 shows a fabrication process flow for a polymer based MEMS supercapacitor.<sup>[21]</sup>

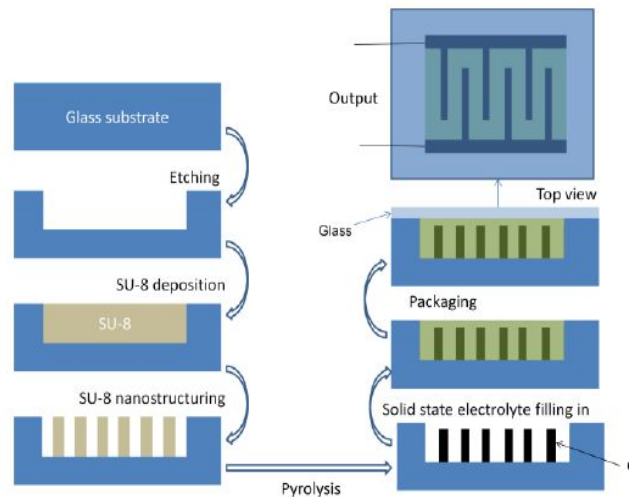


Fig. 1.6 Polymer-carbon based double layer supercapacitor

Firstly, a groove is etched and SU-8 was filled in this groove. then, the Tilted-Exposure Lithography is used to fabricate nanoholes. Thirdly, carbonization process is performed to form 3D carbon structures. Finally, the electrolyte is filled in this structure and supercapacitor is packaged.

### 1.5 State-of-art of MEMS supercapacitors

Suprecapacitors have been studied for over 60 years. And MEMS supercapacitors have been made with advanced designs including the use of high surface area electrodes such as single-walled carbon nanotubes and other high surface area carbons on an industrial front.<sup>[22]</sup> For nanostructure materials in developing supercapacitors, activated carbons, carbide derived carbons, graphene, carbon onions and nanotubes (CNT) had been used for electrode materials. Fig. 1.7 shows a double layer supercapacitor that is fabricated by Y. Q. Jiang.<sup>[23]</sup> The electrode of this supercapacitor is CNTs that was 5mm×7mm with about 30 comb fingers an a single electrode. The specific capacitance density was calculated as 428 $\mu\text{F}/\text{cm}^2$  and power density of 0.28mW $\text{cm}^{-2}$  which is about 1000 times higher than those with plain metal electrodes without CNT forests. In addition, charging and discharging experiments show over 92% efficiency and very strong cycling stability.

## Carbonization of SU-8 based electrode for MEMS supercapacitors

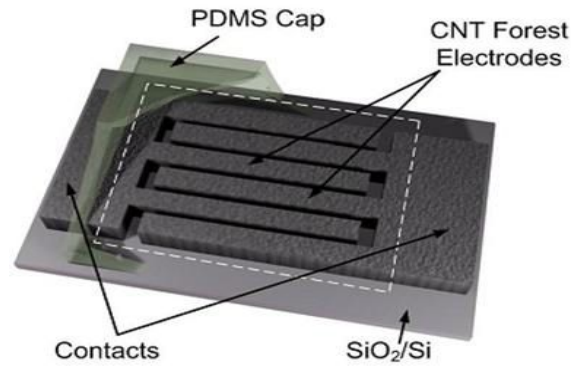


Fig. 1.7 CNT supercapacitor<sup>[23]</sup>

Conducting polymers attracted much attention as electrode materials because of their high electrical conductivity which reduces the internal resistance and high pseudo capacitance. Polypyrrole (PPY)<sup>[24-25]</sup> is a promising conducting polymer for electrochemical energy storage based on its high capacitance and good chemical stability. High flexibility and ease fabrication are important advantages for PPY films.

All-solid-state electrochemical micro supercapacitors have been fabricated by Joo-Hwan Sung et al.<sup>[26-27]</sup> photolithography, electrochemical polymerization and solution casting techniques are used to fabricate the device. The fabrication process flow is shown in Fig. 1.8. The gold layer as current collectors are fabricated by lithography and wet etching process. Then Polypyrrole (PPy) as the electro active material are compounded on the gold layer. The size of the supercapacitor is 2 mm×2 mm, and the capacitance is 2 mF/cm<sup>2</sup>.

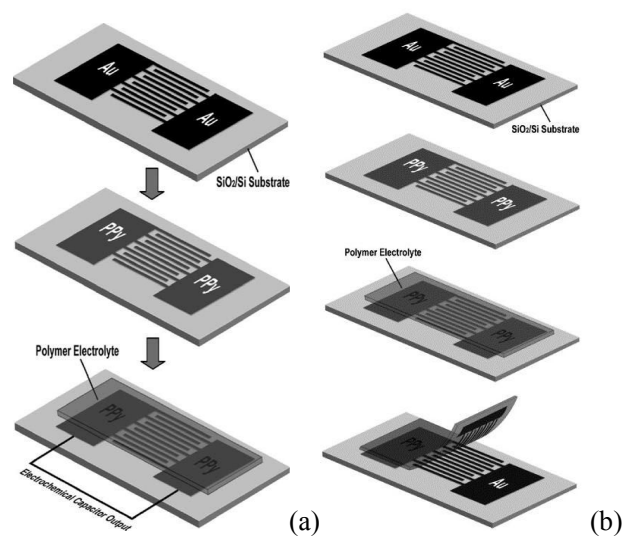


Fig.1.9 Fabrication procedures for (a) micro capacitor on silicon substrate,<sup>[26]</sup> and (b) flexible micro supercapacitors<sup>[27]</sup>

## Carbonization of SU-8 based electrode for MEMS supercapacitors

Tilted-Exposure Lithography has been used for a few years. Manhee Han et al.<sup>[28]</sup> reported a new 3D micro fabrication method with inclined/rotated UV lithography using the thick SU-8 photoresist. It is shown in Fig. 1.10. The resist and a photomask are inclined and rotated to a UV light source to fabricate various 3D microstructures.

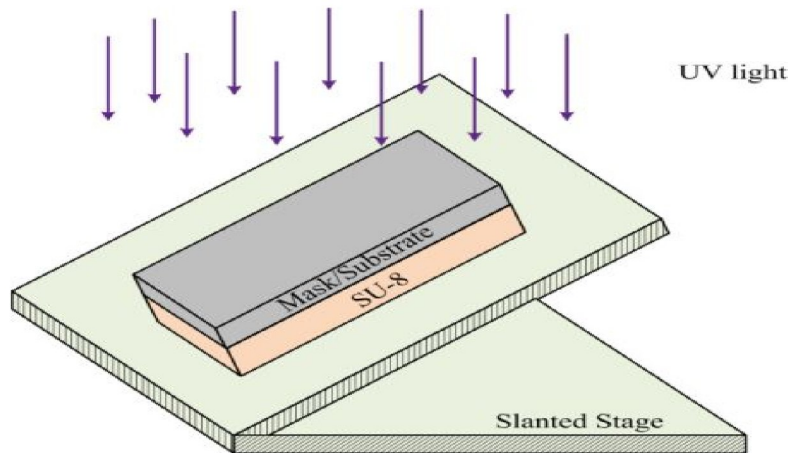


Fig. 1.10 inclined UV exposure<sup>[28]</sup>

C-MEMS technology is used for surface enhancement for fabricating electrodes of supercapacitors. C-MEMS technology can construct 3D carbon microelectrode arrays due to the attractive properties of C, it has mechanical durability, chemical stability and electrical conductivity.

In recent years, MEMS supercapacitor using SU-8, PPY, and all solid electrolyte structure is studied as the target. The electrode material and dielectric layer of supercapacitor is used of chemical vapor deposition (CVD), low pressure chemical vapor deposition to enhance (LPCVD), physical vapor deposition (PVD) to achieve the corresponding thin film deposition. In order to improve the capacity and energy density for MEMS supercapacitors, We need to further study the fabrication process and structural design.

### ***1.6 The topic of this thesis***

In my project, to get electrode of supercapacitors with high adhesion in the substrate after carbonization, my tasks are listed below:

- 1) Building the roots for carbonization of SU-8

## **Carbonization of SU-8 based electrode for MEMS supercapacitors**

---

- 2) SU-8 process for low stress structure of electrodes
- 3) Carbonization process for electrodes of supercapacitors
- 4) Characterization of carbonization process and carbon films

## Chapter 2 Experiments

In this chapter, the system setup for Lithography and system setup for carbonization will be introduced. For building a strong root in the silicon wafer, reactive ion etching technology and wet etching technology are very important in my design.

### *2.1 System setup for lithography*

The steps of photolithography include wafer cleaning, spin coating, soft bake, exposure, post bake, development and hard bake. Baking is an important step for the photolithography process, the baking time and temperature can directly affect other process. Hot plate is used in baking as show in figure 2.1. It provides a stable temperature during the baking.



Fig. 2.1 Hot plate

Photoresist layers of different thickness on the wafer can be deposited with varying spin program. In our lab, the spinner is shown in figure 2.2 that was used in spin coating. By changing the spin steps, speed and spin time in each step, programmed by the programmer of the spinner, the required thickness of the photoresist can be achieved by design the spin program.

## Carbonization of SU-8 based electrode for MEMS supercapacitors

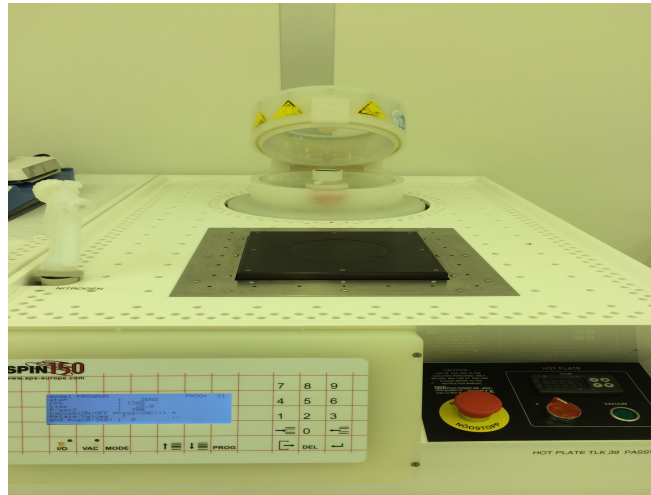


Fig. 2.2 Spinner

The device for exposure process is shown in figure 2.3. The Karl Suss MA 56 is a mask alignment and exposure system which offers unsurpassed, highly economical mass production capabilities for cassette to cassette handling of wafers up to 4 inches wafers and 5 inches masks, although smaller wafers and chips may be mounted to a 4 inches carrier wafer and processed. The light source is a 350 W mercury arc lamp with 365 nm wavelength. The mask and microscope have motorized motion in x and y, and they may be moved together or independently over the stationary wafer.



Fig. 2.3 Mask Aligner Karl Suss MA56

When finish development, we need to measure the thickness of the microstructures and observe the morphology of structure. DEKTAK Profilometer is used for thickness

## Carbonization of SU-8 based electrode for MEMS supercapacitors

measurement with a vertical resolution of 1nm, it is shown in figure 2.4. Optical Microscope I Leica DM4000M is very useful to observe the morphology of structure and do some analysis. This microscope is shown in figure 2.5 that supply 6x objective turret is equipped with following objectives 2.5x,5x,10x,20x,50x and 100x, and is coded so that the objective used is immediately detected.



Fig. 2.4 DEKTAK Profilometer

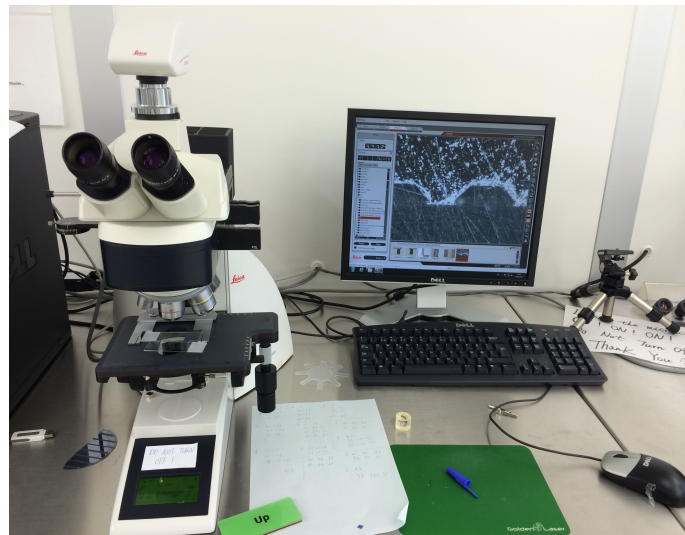


Fig. 2.5 Microscope I Leica DM4000M

### 2.2 System setup for carbonization

Furnace is the key in carbonization process, high temperature vacuum tube furnace GSL-1100 is used in my experiment. GSL-1100 series high temperature vacuum tube furnace is a compact designed for heating samples up to 1100 °C. Stainless steel vacuum flange with valve, vacuum gauge and quartz tube are included for immediate use. Built in precision temperature controller is able to program the heating rate, dwell time and cooling rate up to 30 segments. The furnace can be set up in both vertical and horizontal position to meet various applications. As shown in figure 2.6, It is excellent for annealing, diffusing and sintering sample in various atmospheres.

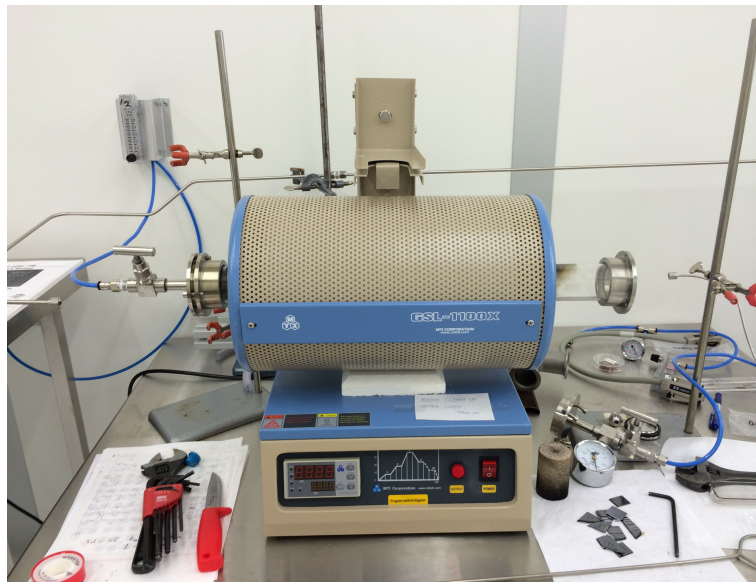


Fig. 2.5 High temperature vacuum tube furnace GSL-1100

Carbonization process is a pyrolysis process for decomposing organic materials by heating in the absence of oxygen. During the carbonization process, inert gas environment should be provided to prevent the presence of oxygen. The inert gas is mixed-gas(95% N<sub>2</sub> and 5% H<sub>2</sub>), and the gas flow into the furnace with a constant flow meter. Figure 2.6 shows the temperature controller panel.



Fig. 2.6 Temperature controller panel

The features of the high temperature furnace is shown in table 2.

Table 2. Features of furnace

Power:1200W
Operating Voltage: 220V AC±10% Single Phase
Single Phase, 50/60 Hz
Operating Temp Range C: 200 °C ~1100 °C
Temperature accuracy: +/- 10 °C
Suggested Normal Heating Rate: ≤10 °C /min
Max. Heating Rate: ≤ 30 °C /min
Temperature control: 30 segments programmable digital controller with PID
function and overheated and overloaded protection
Quartz Tubes size (inch): 2" O.D x 1.7" I.D x 24" L

### ***2.3 RIE technology***

Reactive ion etching (RIE) is an etching technology used in microfabrication. This process involves both physical and chemical reactions to etch off the silicon and achieve high levels of resolution. The plasma is generated under low pressure (vacuum) by an electromagnetic field. High-energy ions from the plasma attack the wafer surface and react with it. According to the morphology of the etched structure, we can divide it into two groups. one is isotropic etch, another is anisotropic, can be seen in figure 2.7 and figure 2.8.<sup>[29]</sup>

## Carbonization of SU-8 based electrode for MEMS supercapacitors

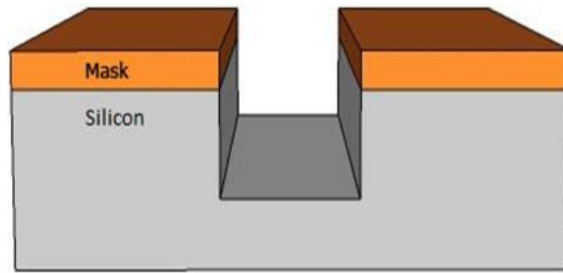


Fig. 2.7 Anisotropic etching

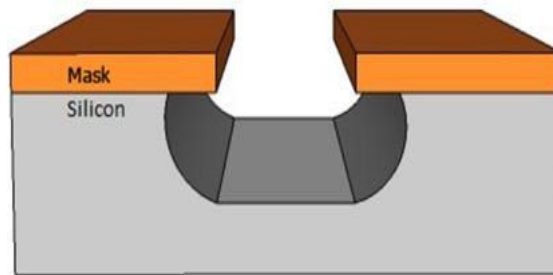


Fig. 2.8 Isotropic etching

In the RIE process, positive ions are produced from reactive gases which are accelerated with high energy to the substrate and chemically react with the silicon. The common RIE gases for Si are  $\text{CF}_4$ ,  $\text{SF}_6$  and  $\text{BCl}_2 + \text{Cl}_2$ . Figure 2.9 shows the Reactive Ion Etcher that was used in my experiment.



Fig. 2.9 Reactive Ion Etcher

## ***2.4 Wet etching technology***

Wet etching means to remove materials from wafer that process uses liquid chemicals or etchants. The patterns are defined by masks on the wafer. Materials that are not protected by the masks will be etched away by liquid chemicals. We can describe the wet etching process in three steps: (1) Diffusion of the liquid etchant to the structure that is to be removed. (2) The reaction between the liquid etchant and the material being etched away, this reaction produce the oxidation of the material then dissolving the oxidized material. (3) the byproducts diffuse in the reaction from the reacted surface.

According to different etchants, wet etching also can be divided into two categories. Isotropic wet etching process use acidic etchants, etching morphology is shown in figure 2.10.<sup>[29]</sup> For isotropic wet etching silicon, a mixture of hydrofluoric acid, nitric acid, and acetic acid (HNA) is the most common etchant. Anisotropic wet etching process use alkaline etchants, liquid etchants etch crystalline materials at different rates depending on which crystal face is exposed to the etchant. As figure 2.11<sup>[29]</sup> shows result that etch the 100 oriented silicon wafer. The anisotropic wet etching agents for silicon are potassium hydroxide (KOH), ethylenediamine pyrocatechol (EDP), and tetramethylammonium hydroxide (TMAH).

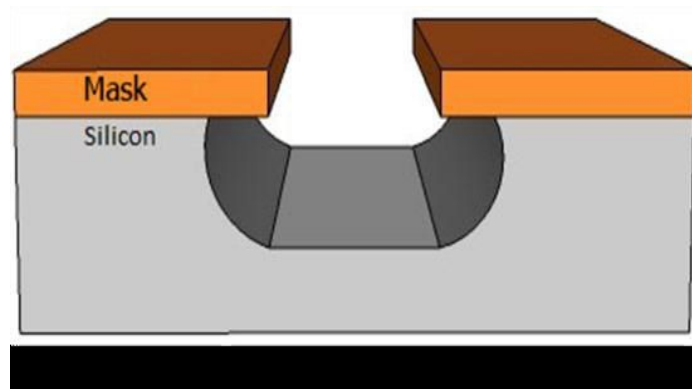


Fig. 2.10 Isotropic wet etching

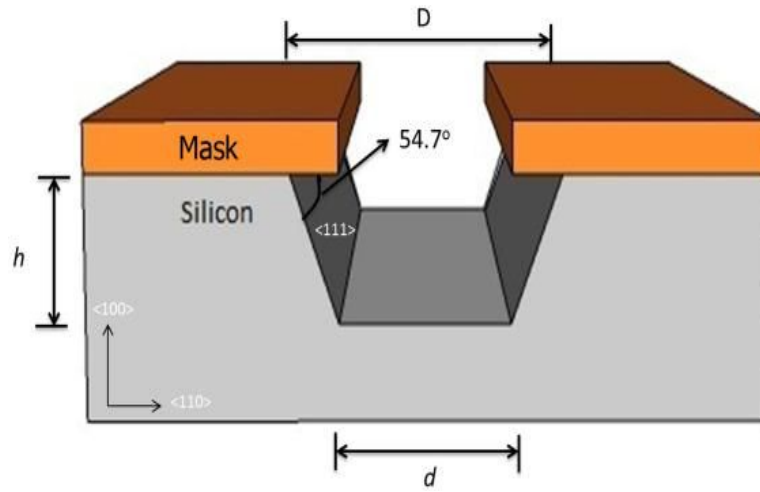


Fig. 2.11 Anisotropic wet etching

The relationship between mask dimensions, etch depth and the floor width is given in equation 2-1.

$$d = D - 2h \cdot \cot(54.7^\circ) \quad (2-1)$$

## Chapter 3 Micro Mechanical Interlocking

In this chapter, micro mechanical analysis of three different structures into the substrate surface are discussed. We will find the best structure for increasing adhesion between the material and substrate, and design the micro fabrication process for this structure. This structure will be the root for SU-8 electrode structure.

### *3.1 Analysis of Micromechanical interlocking as the root*

We could understand adhesion that can be defined as a force which applied to the interface between two materials to join them together and resist separation. According the mechanisms of adhesive bonding, it can be classified under six distinct categories: adsorption, electrostatic, diffusion, chemical bonding, weak boundary layer effects, and mechanical interlocking. For my project design, in order to ensure the SU-8 electrode structure locks firmly in the wafer when finish carbonization process, the mechanical interlocking is the best choice as the root for SU-8 electrode structure.

Micro mechanical interlocking is built by penetrating a material into some configurations of the irregular pits in the surface of the substrate. Micro mechanical interlocking of the material into the irregularities of substrate surface provide the major interfacial adhesion. The irregularity of substrate surface could be divided into three models as depicted in figure 3.1.<sup>[30]</sup> We assume these three pits have smooth substrate surface, these pits produce mechanical constraint to adhesive materials, which prevent material to peel off from substrate and make two different materials join stronger.

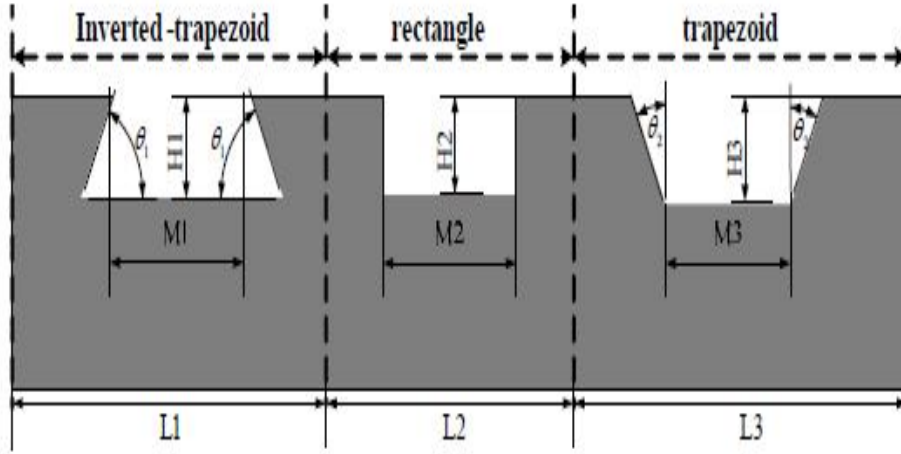


Fig. 3.1 Cross-section schematic of the irregularity of the substrate surface

When the materials fill into the pits, at the same time, the adsorption caused by interfacial van der Waals bonds between molecules of materials and substrate, and also can play an indirect important role to the adhesion.

The van der Waals force can be expressed as follows:

$$F_v = \frac{SA}{6\pi d^3} \quad (3-1)$$

Where A is Hamaker constant, d is the distance of two contact surfaces and S is the contact area. Under similar conditions, the adhesion will increase as the increase of contact area .

As figure 3.1 shows geometric parameters of three types pits, we assume that the following condition holds:

$$M_1 = M_2 = M_3 \quad (3-2)$$

$$L_1 = L_2 = L_3 \quad (3-3)$$

$$H_1 = H_2 = H_3 \quad (3-4)$$

Assuming the area of vertical sidewall is M, the bottom area of the pit is N. Under these conditions, we can obtain contact surface area:

$$S_1 = N + \frac{2M}{\sin \theta_1} + 2M \cdot \cot \theta_1 \quad (3-5)$$

## Carbonization of SU-8 based electrode for MEMS supercapacitors

---

$$S_2 = N + 2M \quad (3-6)$$

$$S_3 = N + \frac{2M}{\cos \theta_2} - 2M \cdot \tan \theta_2 \quad (3-7)$$

Where  $\theta_1$  and  $\theta_2 \in [0, 90]$ ,  $\theta_1$  and  $\theta_2$  is the inclination angle for inverted-trapezoid and trapezoid, respectively.

$$\begin{aligned} S_1 &= N + 2M \cdot \frac{1 + \cos \theta_1}{\sin \theta_1} \\ &= N + 2M \sqrt{\frac{(1 + \cos \theta_1)^2}{\sin^2 \theta_1}} \end{aligned} \quad (3-8)$$

Because of  $(1 + \cos \theta_1) / \sin \theta_1$  is always greater than 1 or equal to 1, so  $S_1 \geq S_2$ .

$$\begin{aligned} S_3 &= N + 2M \cdot \frac{1 - \sin \theta_2}{\cos \theta_2} \\ &= N + 2M \cdot \sqrt{\frac{(1 - \sin \theta_2)^2}{1 - \sin^2 \theta_2}} \\ &= N + 2M \cdot \sqrt{\frac{1 - \sin \theta_2}{1 + \sin \theta_2}} \end{aligned} \quad (3-9)$$

Because of  $(1 - \sin \theta_2) / (1 + \sin \theta_2)$  is always less than 1 or equal to 1, so  $S_3 \leq S_2$ .

From the above equation we obtain  $S_1 \geq S_2 \geq S_3$ , and further we also can get  $F_1 \geq F_2 \geq F_3$ . All analysis above shows that the inverted-trapezoid in substrate is the most favorable structure to the improvement of the adhesion, rectangle take second place, trapezoid the poorest. Geometric parameters for each structure of three also can be optimization, because all kinds of structure is easy to produce stress concentration which could result in fracture in the internal of material. Especially, inverted-trapezoid structure can give the best adhesion, but it is also the easiest to produce larger stress concentration than others. For inverted- trapezoid structure, we must carefully design parameters to achieve the maximal degree improved adhesion.

### ***3.2 Fabrication process design for inverted-trapezoid pit***

In order to fabricate inverted-trapezoid pit in the silicon wafer, we must combine the technology of dry etching and wet etching. The mechanism of fabrication inverted-trapezoid pit is that different etching rate occurs in different crystal surface. Table 4 and 5 shows the result of etching rate<sup>[31-32]</sup>.

Table 4. Anisotropic KOH etching rates

Crystallographic Orientation	Rates at different KOH Concentration		
	30%	40%	50%
100	0.797	0.599	0.539
110	1.455	1.294	0.870
210	1.561	1.233	0.959
211	1.319	0.950	0.621
221	0.714	0.544	0.322
111	0.005	0.009	0.009

Table 5. Silicon orientation-dependent etch rates of TMAH

Crystallographic Orientation	Rates at 20% TMAH
100	0.603
110	1.114
210	1.154
211	1.132
221	1.142
111	0.017

we could find that the 110 plane is the fastest etching primary surface from table 4 and 5. Because the ideal 110 surface has a more corrugated atomic structure than the 100 and 111 primary surfaces, this atomic structure reaction with etchant occurs more easily. The 111 plane is an extremely slow etching plane that is tightly packed. This

## Carbonization of SU-8 based electrode for MEMS supercapacitors

plane has a single dangling-bond per atom, and is overall atomically flat. The atomic structure of different crystal orientation is shown in figure 3.2<sup>[34]</sup>.

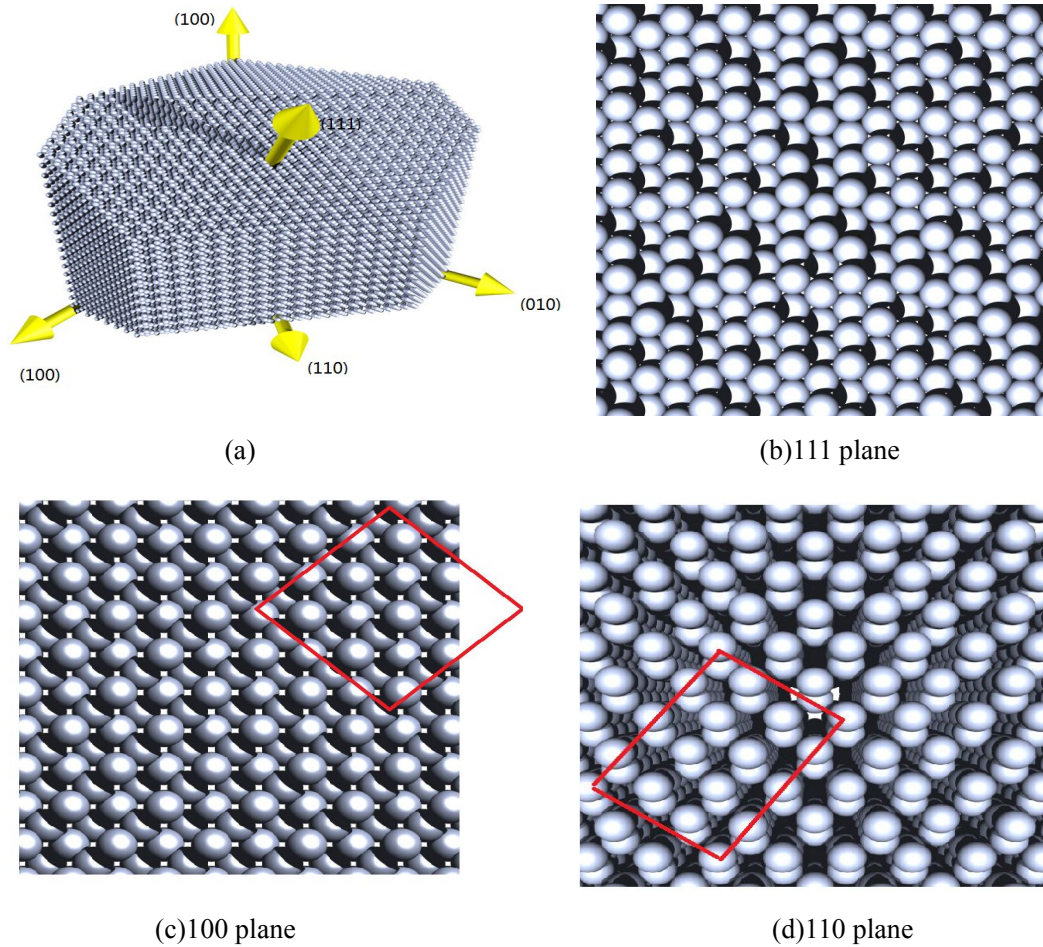


Fig. 3.2 The atomic structure of different crystal orientation

From the above analysis, the fabrication process for inverted-trapezoid pit can be design that is shown in figure 3.3. First, we use the silicon wafer that is coating with  $\text{SiO}_2$  on one side surface, the orientation of silicon wafer is  $\langle 100 \rangle$ . Photolithography process is used to obtain the pattern in photoresist. Then, etch  $\text{SiO}_2$  that is exposed portions, anisotropic dry etch Si. When finish these process, the orientation of the top view surface is  $\langle 100 \rangle$ , and the orientation of the side wall is  $\langle 110 \rangle$ . Finally, anisotropic wet etch Si, because of  $\langle 110 \rangle$  surface has the fastest etching rate, etching for the side wall will be faster than bottom. When orientation of the side wall turn into  $\langle 111 \rangle$  by the etching process, the etching will stop. So we can get the inverted-trapezoid pit from this method.

## Carbonization of SU-8 based electrode for MEMS supercapacitors

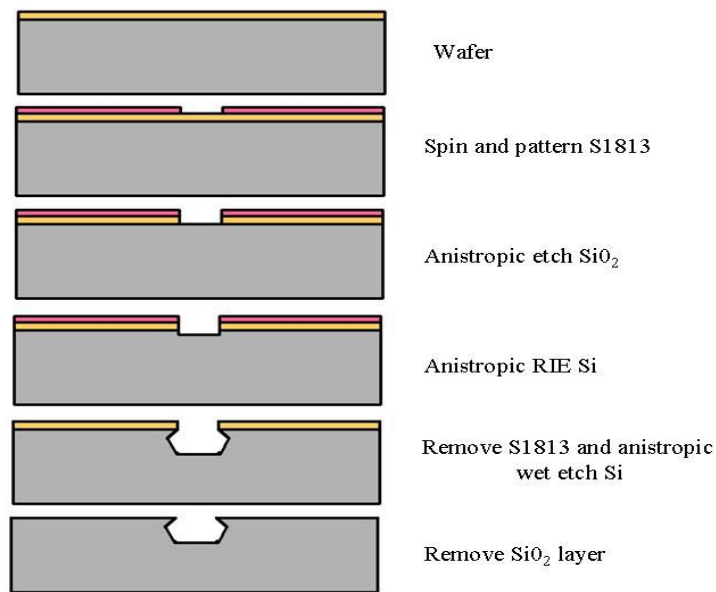
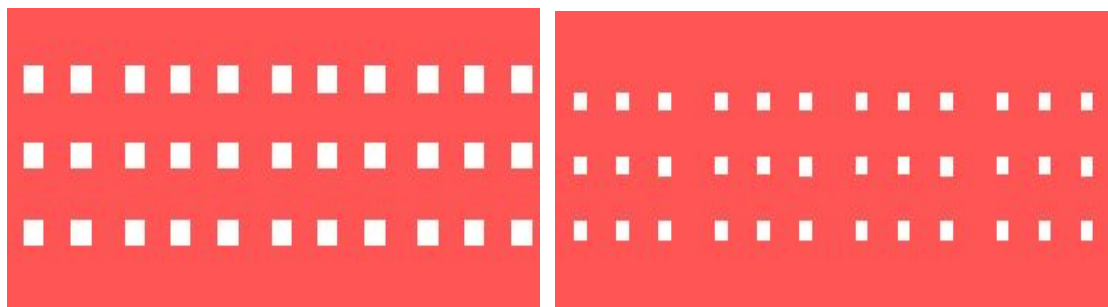


Fig. 3.3 the fabrication process for inverted-trapezoid pit

Based on the function of pit is to improve the adhesion between the SU-8 structure and silicon wafer, the shape of the opening is designed to square structure. So the mask for the shape of the opening is shown in figure 3.4. The dimension of opening are 100 $\mu\text{m}$  and 150 $\mu\text{m}$ , respectively.



(a) 3 rows 150\*150 $\mu\text{m}$  square structure

(b) 3 rows 100\*100 $\mu\text{m}$  square structure

Fig. 3.4 mask design for root

## Chapter 4 Fabrication Process of Inverted-trapezoid Pit

Inverted-trapezoid pit is very important for SU-8 electrode structure, ensure SU-8 electrode structure to be locked in the substrate when finish carbonization process. In this chapter, we will discuss fabrication process of inverted-trapezoid pit. Based on the experimental results, analyze the critical step, and identify the influencing factors for this process.

### 4.1 *Photolithography process*

According the analysis in chapter 3, the <100> silicon wafer that is grown with 400nm~500nm SiO<sub>2</sub> is used in my experimental. A common lithography process is shown in below:

1. Wafer cleaning. Before the start of the experiment, There may be dust, lint, bacteria, water and oil on the wafer. These impurities can affect the result of spin coating.

2. Dehydration of wafer. This operation promotes adhesion of the photoresist by evaporating any residual moisture on the surface of the wafer. The dehydration bake can be performed on an aluminum foil that is placed on hotplate for a few minutes.

3. Spin coating. the photoresist bonds uniformly to the surface of wafer, with excess flying off during spinning process.

4. Soft bake. The purpose of the soft bake is hardening the photoresist, it is a simple process of heating the surface on hot plate.

5. Exposure. This process transfers the pattern from the mask to the photoresist film.

6. Post bake. The post exposure bake (performed after exposure, but before development) can be applied above the softening point of the resist without destroying

## Carbonization of SU-8 based electrode for MEMS supercapacitors

the structures to be developed due to the still closed resist film. In some case, post bake should be applied, such as, chemically amplified resists, cross linking negative resists and highly reflective substrates.

7.Development. Chemicals are applied to decompose the non-polymerized sections of the resist. This process leaves the photoresist structure that is required.

8.Hard bake. Hard bakes are normally not required. For cross link the material, hard bake certainly can improve the strength of the devices.

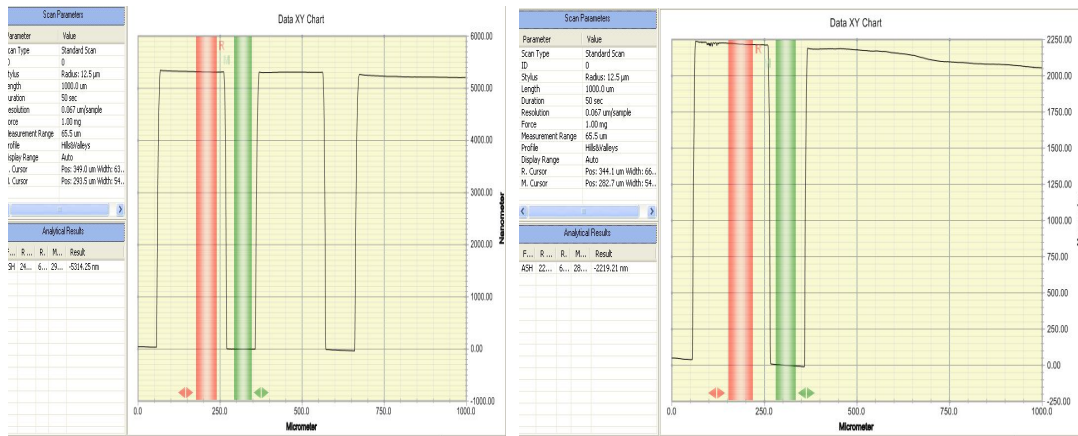
In my experiments, the positive photoresist S1813 and S1828 are used in this process. The first attempt, two wafers use photoresist S1813 and S1828, respectively. The process details are given in table 6.

Table 6.Photolithography process of first attempt

Wafer 1	Wafer 2
Wafer cleaning	Wafer cleaning
Dehydration	Dehydration
Spin-coat:	Spin-coat:
Photoresist 1828, Spin speed 1000rpm for 35s (4.9um)	Photoresist 1813, Spin speed 1000rpm for 35s (1.8um)
Soft bake: 90°C for 2mins	Soft bake: 90°C for 2mins
Cool down: for 5mins	Cool down: for 5mins
Exposure: for 40seconds	Exposure: for 40seconds
Development: for 30seconds	Development: for 30seconds

When finish photolithography process, as the design in chapter 3 shows, we need etch SiO<sub>2</sub> that is exposed portions. HF solution is used to etch SiO<sub>2</sub> for 10mins. Figure 4.1 shows the thickness of the pit that was measured after etching SiO<sub>2</sub>. And figure 4.2 shows the top view of the opening.

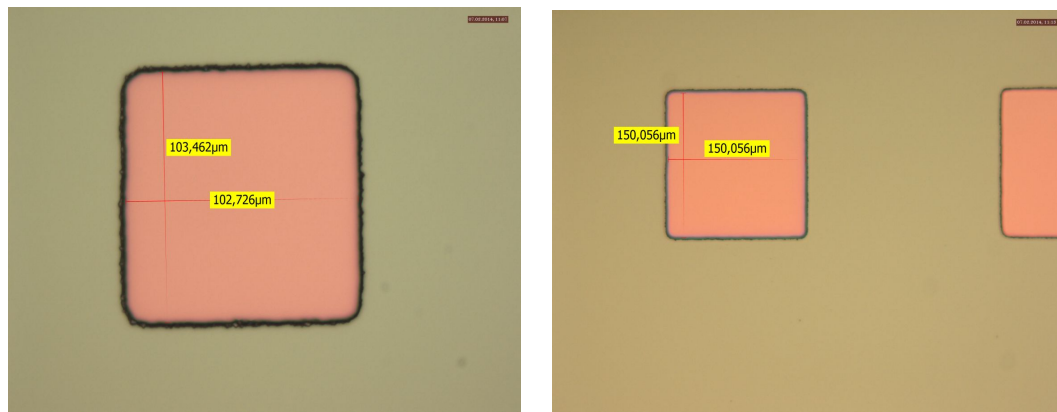
## Carbonization of SU-8 based electrode for MEMS supercapacitors



(a) wafer 1 after etching SiO<sub>2</sub>

(b) wafer 2 after etching SiO<sub>2</sub>

Fig. 4.1 thickness after etching SiO<sub>2</sub>



(a) 100μm square structure

(b) 150μm square structure

Fig. 4.2 top view of structure

As figure 4.1 shows the thickness of structure in wafer1 is 5.3μm, and in wafer 2 is 2.2μm. Before etching SiO<sub>2</sub>, the thickness of photoresist are 4.9μm and 1.8μm. After calculating, we can get the thickness of SiO<sub>2</sub> is about 0.4μm. This result conform with the providing thickness of SiO<sub>2</sub> (400nm~500nm). The opening dimension of structure is almost same with the design.

### 4.2 Anisotropic RIE etching process

Reactive ion etching is key to obtain inverted-trapezoid pit in my design. We have to ensure the sidewalls flat as much as possible, so the Perfect <110> plane will lead to inverted-trapezoid structure when finish wet etching silicon.

### 4.2.1 Factors of RIE etching process

In my experiments, SF<sub>6</sub> and O<sub>2</sub> are chosen for RIE etching of silicon. Each gas has its own specific function in etching process, changes to the etch profile can be controlled by altering the flow rate of one of the gases. The SF<sub>6</sub> and O<sub>2</sub> generate F and O free-radicals under the influence of strong electric fields. The F radicals initiate a chemical reaction with silicon, producing the highly volatile byproduct SiF<sub>4</sub>, and the O radicals will cause passivation of the silicon surface by forming SiO<sub>x</sub>F<sub>y</sub>. SF<sub>6</sub> is also can provide SF<sub>x</sub><sup>+</sup> ions, which act to remove the oxyfluoride layer. Along with the etching process, substrate damage and mask erosion will appear. This problem can be minimized through appropriate lowering of ion energy. Etch profile is also controlled at lower ion energies. Ion energy is governed by the dark space voltage D<sub>v</sub>. The relationship between D<sub>v</sub> and etching parameters can be expressed as<sup>[35]</sup>:

$$D_v \propto \frac{P_{RF} \cdot F[O_2]}{p \cdot F[SF_6]} \quad (4-1)$$

Where p is system pressure, F[*gas*] is the flow rate. When RF power, system pressure and gas flow rates are at the right levels, etch features with vertical side walls will be generated.

By changing the ratio of SF<sub>6</sub> and O<sub>2</sub> to control the etch rate and etch profile is an effective and simple method. Keeping the SF<sub>6</sub> flow rate is constant, the system pressure is set at 30 and 200mTorr, respectively. The effect of increments in oxygen concentration on etch rate is demonstrated in figure 4.3. From figure 4.3, we could find an increase in silicon etch rate up to a maximum at the beginning, and follow the oxygen concentration increasing, the etching rate will decrease. The maximum etch rate is approximately twice that of the minimum value when the system pressure is set at 200mTorr. Obviously, the greater pressure corresponds greater etch rate. But faster etching rate is not necessarily beneficial for for the etching profile.

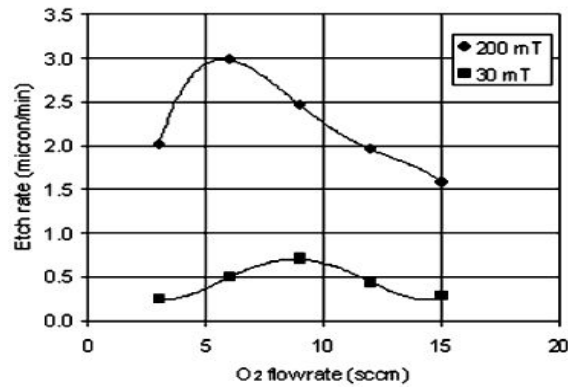


Fig. 4.3 Si etch rate dependency on O<sub>2</sub> flow rate

The effect of oxygen concentration on silicon etch profile is shown in figure 4.4. Keeping the SF<sub>6</sub> flow rate and system pressure are constant at 12sccm and 200mTorr, respectively. And RF power is 160 W. In figure 4.4(a), silicon etch profile is largely isotropic. As the oxygen flow rate increase to 6sccm, the degree of isotropy is reduced. At an oxygen flow rate of 9sccm (Fig. 3c), the overall degree of side-walls close to 90° with respect to the horizontal. When the oxygen flow rate is 12sccm, the side-walls exhibit a positive taper.

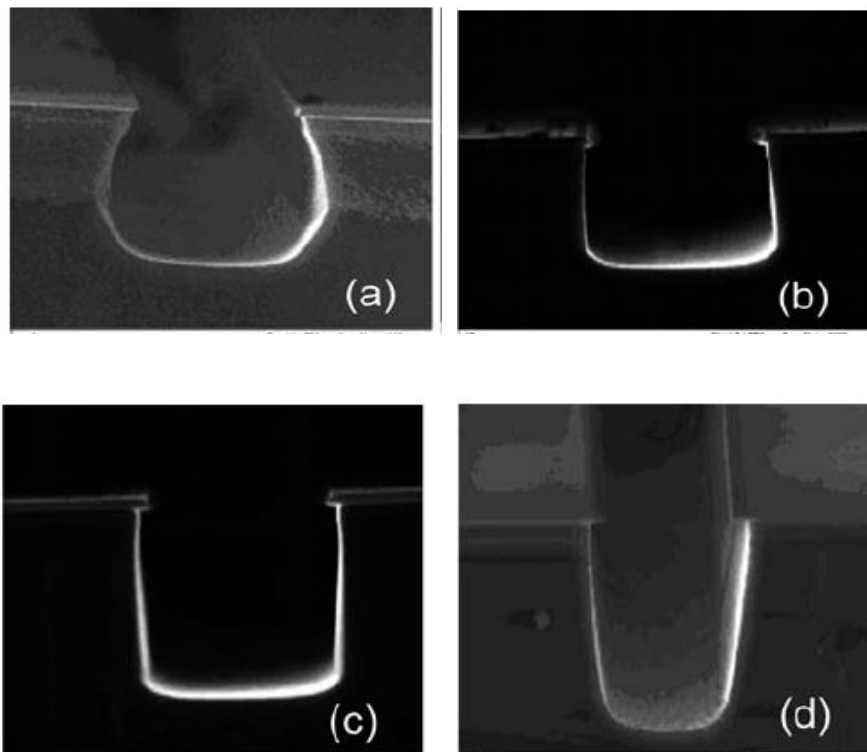
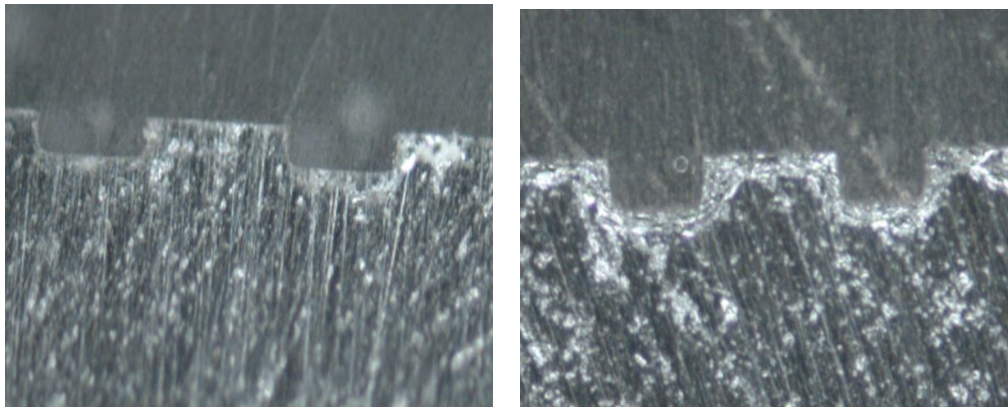


Fig. 4.4 Etch profile at different O<sub>2</sub> flow rates, (a) 4sccm, (b) 6sccm, (c)9sccm, (d)12sccm

## **Carbonization of SU-8 based electrode for MEMS supercapacitors**

At high pressures and high O<sub>2</sub> flows, in the anisotropic etching regime, the etch surface roughness increases. CHF<sub>3</sub> can be added into an SF<sub>6</sub>/O<sub>2</sub> gas mixture improves the etch surface quality<sup>[42]</sup>, as shown in figure 4.5. Etching parameters is 10sccm O<sub>2</sub>, 30sccm SF<sub>6</sub>, 12sccm CHF<sub>3</sub>, 100mTorr pressure and 150W RF power. Surface roughness of figure 4.5(a) is significantly less than (b). But the addition of CHF<sub>3</sub> results in smooth surfaces, only slightly affecting the anisotropy etching. At high CHF<sub>3</sub> flows, the anisotropy will be reduced and more isotropic etching is obtained.



(a) etching with CHF<sub>3</sub>

(b) etching without CHF<sub>3</sub>

Fig. 4.5 Comparison of surface roughness after RIE etching

From the above results, by controlling the parameters of the RIE etching and adding a suitable CHF<sub>3</sub> gas, we can get a good RIE etching result that will have a direct impact on the morphology of structure.

### **4.2.2 Experimental procedures and results**

Considering the large number of RIE etching test, we cut the wafer 1 and wafer 2 into many small pieces. Through repeated attempts, the basic anisotropic RIE etching parameters is listed in the table 7 for my experiment. Under this setting, Etch profile is almost close to anisotropy etching, ensure next step is carried out smoothly.

## Carbonization of SU-8 based electrode for MEMS supercapacitors

Table 7. RIE etching parameters

Flow rate of O <sub>2</sub> (sccm)	Flow rate of SF <sub>6</sub> (sccm)	Pressure(mTorr)	RF Power(W)
10	30	100	150

Since the thickness of photoresist is 1.8 $\mu$ m on wafer 2, it is too thin as the mask during the etching. When the etcher is working for 15 minutes, photoresist and SiO<sub>2</sub> layer have been destroyed. Figure 4.6 shows the wafer 2 after RIE etching, photoresist and SiO<sub>2</sub> layer are removed by the etching process, Black Silicon appears on this wafer.



Fig.4.6 wafer 1 RIE etching for 15mins

In order to obtain deeper anisotropic RIE etching, spin coating thicker photoresist is required on the wafer. So wafer 2 fails in this process. And table 8 shows the thickness of wafer 1 after RIE etching, etching rate is approximately 0.9 $\mu$ m/min.

Table 8. Wafer 1 thickness after RIE etching

Etching time	5mins	10mins	15mins	20mins	25mins
Etching depth	4.5 $\mu$ m	9 $\mu$ m	12 $\mu$ m	17 $\mu$ m	23 $\mu$ m

## Carbonization of SU-8 based electrode for MEMS supercapacitors

Three new wafers are prepared for wet etching Si. Lithography process is repeated, and the photoresist(1828) thickness is 4.6 $\mu$ m. These three wafers use different etching time in RIE etching process, they are named wafer 4, wafer 5 and wafer 6, respectively. Table 9 list the information of these wafers after RIE etching process.

Table 9. Information of RIE etching for new wafers

	Wafer 4	Wafer 5	Wafer 6
Etching time	15mins	20mins	25mins
Etching depth	13 $\mu$ m	17 $\mu$ m	23 $\mu$ m
Addition	12sccmCHF <sub>3</sub>	No	No

### 4.3 Anisotropic wet etching Si

Before wet etching Si process beginning, the photoresist should be remove by S1828 remover. According to the analysis of chapter 2 and chapter 3, 20% TMAH as the Etchant is used in this process at 80°C. Etching time for wafer 4 is 60mins, the etching depth is 78 $\mu$ m7. Figure 4.7 shows the cross section and top view of pit. The RIE etching depth is 13 $\mu$ m from table 9, the depth of inverted-trapezoid is 12.007 $\mu$ m from figure 4.7(a), this result is consistent with the design. The angle of this inverted-trapezoid and horizontal surface is 54.6°, it is very close to 54.7°, that means the orientation of the side wall is <111>surface, and etching Si process has ended in side wall. So we successfully obtain inverted-trapezoid structure.

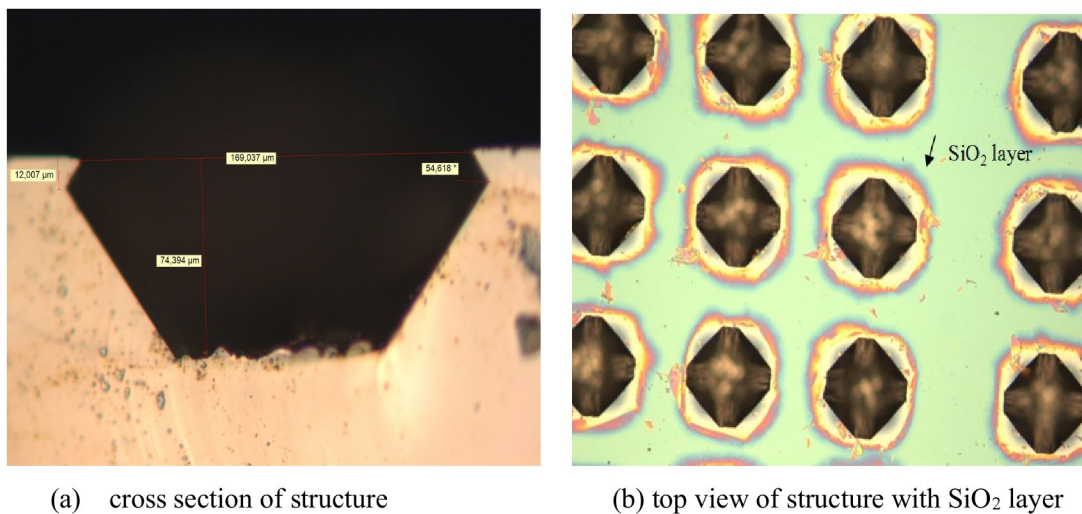
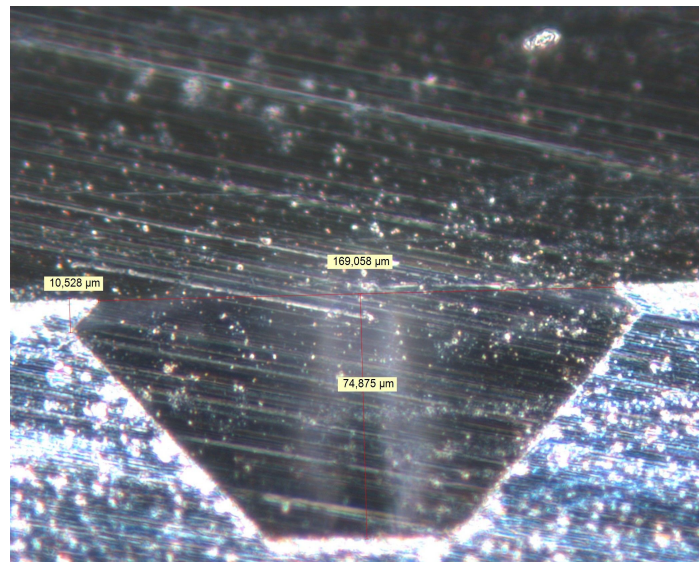


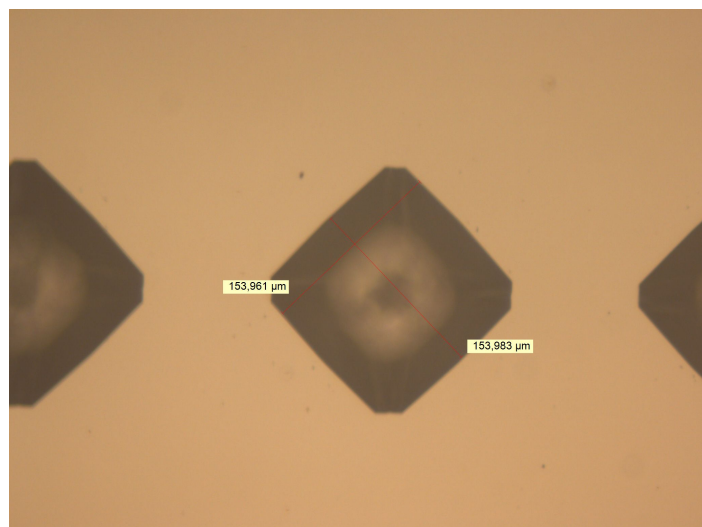
Fig. 4.7 wafer 4 after wet etching Si

## Carbonization of SU-8 based electrode for MEMS supercapacitors

Figure 4.8 shows wet etching result of wafer 5. Etching time for wafer 5 is 60mins, and etching depth is 77 $\mu$ m that is measured by Profilometer. As the figure shows, thickness of inverted-trapezoid is 10.5 $\mu$ m that is less than depth of RIE etching 17 $\mu$ m. Causing this problem may be due to the sidewall surface is not overall vertical when finish RIE etching process, so the bottom of sidewall is not  $\langle 110 \rangle$  orientation, this will directly affect the results of wet etching. Furthermore, the dimension of opening is more than design after wet etching Si. That is because mask undercut occurs during the etching process, then remove mask layer, so the actual opening size is more than design.



(a) cross section of structure

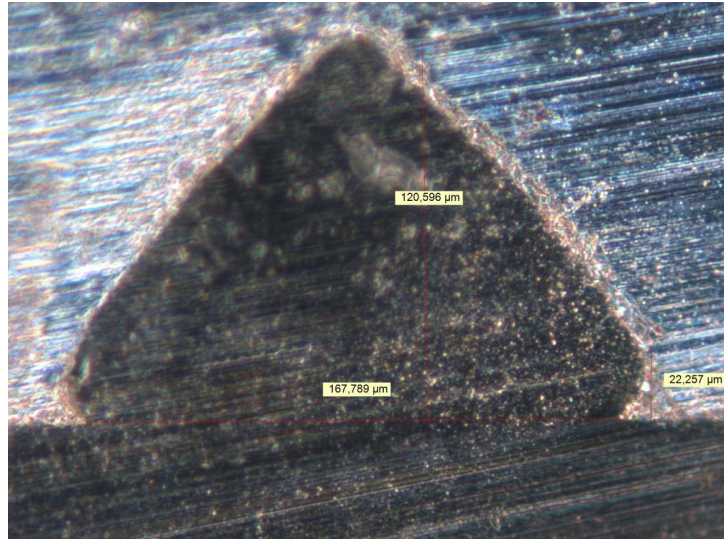


(b) top view of structure

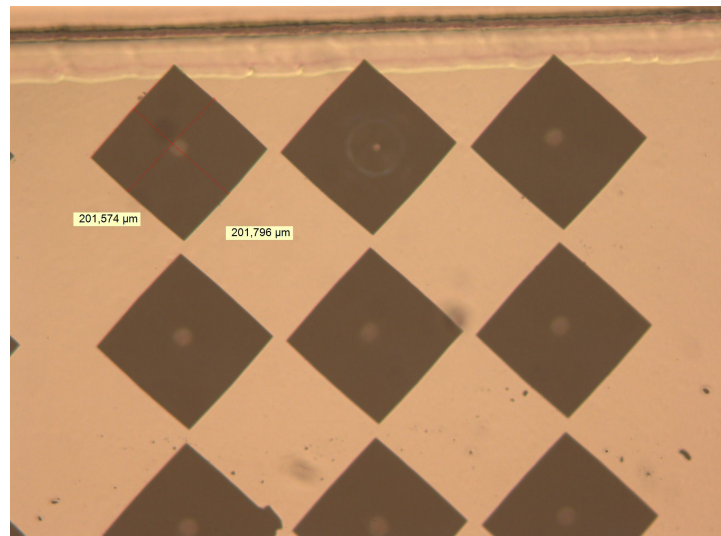
Fig. 4.8 wafer 5 after wet etching Si

## Carbonization of SU-8 based electrode for MEMS supercapacitors

Comparison of wafer 4 and wafer5, wafer 6 has more etching time. The thickness of final pit is 122um for etching time 120mins. As figure 4.9(a) shows, the etching has completed, the bottom of pit is tapered structure. Thickness of inverted-trapezoid is 22.3um.



(a) cross section of structure



(b) top view of structure

Fig. 4.9 wafer 6 after wet etching Si

Inverted-trapezoid pit is fabricated successfully by these process. But note that alignment when doing exposure process, there has an angle of  $45^\circ$  between  $\langle 110 \rangle$  surface and  $\langle 100 \rangle$  surface. For  $\langle 100 \rangle$  silicon wafer, we must ensure square structure on mask has a rotation angle of  $45^\circ$  with wafer, so that  $\langle 110 \rangle$  surface could be obtained in the subsequent step.

## Chapter 5 Carbonization of SU-8 based Electrodes

In this chapter, these wafers with inverted-trapezoid pit spin coating SU-8 photoresist, and pattern different size of electrode structure by the second mask. The property of SU-8 is analyzed for carbonization process design. Carbonization process is performed in high temperature furnace and it is a self-built pyrolysis system.

### *5.1 SU-8 technology based on MEMS Supercapacitor*

Supercapacitor as energy storage devices has been introduced in chapter 1. In order to improve capacity of supercapacitor, increase the contact area of the electrode with the electrolyte is an effective approach under other factors remain unchanged. However, SU-8 is used as the material of electrode in this project, fabricate high aspect ratio microstructure by SU-8 process as the electrodes that is applied.

#### **5.1.1 SU-8 photoresist**

SU-8 is a commonly used epoxy-based negative photoresist for micro machining and other microelectronic applications. It has acid-labile groups and a photoacid generator.<sup>[36]</sup> The main components of SU-8 are a Bisphenol A Novolak epoxy oligomer, and about 10 wt% triarylsulfonium hexafluoroantimonate salt photoacid generator, that is shown in figure 5.1. Upon exposure, the photoacid generator decomposes to form hexafluoroantimonic acid that protonates the epoxides on the oligomer. oxonium ions that was protonated will react with neutral epoxides by a series of cross-linking reactions after heating.<sup>[37]</sup> Eight reactive epoxy sites are afforded in each monomer molecule as shown in figure 5.1<sup>[36]</sup>, after photo thermal activation giving a negative tone, the high degree of cross-linking can be obtained. The high mechanical and thermal stability of the lithographic structures will be obtained after this process.

## Carbonization of SU-8 based electrode for MEMS supercapacitors

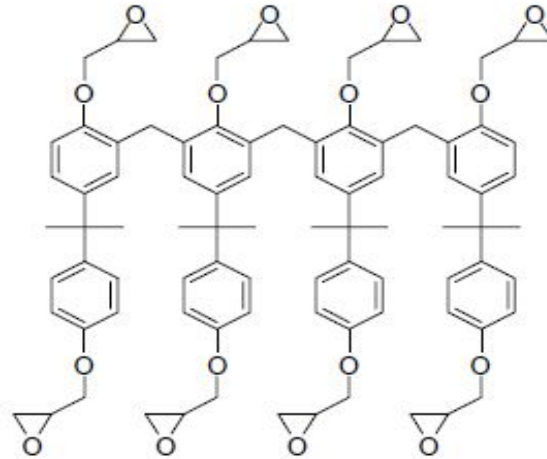


Fig.5.1 Chemical structure of the Bisphenol A Novolak epoxy oligomer contained in SU-8

SU-8 is a high viscous polymer, so it can be spun the thickness of film from 1 micrometer to >200 micrometer with single spin coating process, and still can be processed by standard contact lithography. SU-8 has very high optical transparency above 360nm, which makes it very favorable for imaging near vertical sidewalls in thick films. Table 10<sup>[38]</sup> lists physical properties of the SU-8 photoresist.

Table. 10 physical properties of the SU-8

Property	Value
Young's modulus, E (post-bake at 95°C)	4.02GPa
Young's modulus, E (hard bake at 200 °C)	4.95 ± 0.42GPa
Biaxial modulus of elasticity, E/(1 - ν)	5.18 ± 0.89GPa
Film stress (post-bake at 95 °C)	16-19MPa
Maximum stress (hard bake at 200 °C)	34MPa
Friction coefficient (post bake at 95°C)	0.19
Glass temperature, Tg (unexposed)	~ 50°C
Glass temperature, Tg (fully cross-linked)	>200°C
Degradation temperature (fully cross-linked)	~ 380°C
Thermal expansion coefficient (post-bake at 95°C)	52 ± 5.1 ppm K <sup>-1</sup>
Polymer shrinkage upon cross-linking	7.5%

## Carbonization of SU-8 based electrode for MEMS supercapacitors

There are two SU-8 types( SU-8 100 and SU-8 2150) that are used in my experiment. Table 11<sup>[39-40]</sup> shows the typical values of the processing parameters for SU-8 100 and SU-8 2150.

Table. 11 processing parameters of SU-8

SU-8 type	SU-8 100	SU-8 2150
Viscosity(cSt)	51500	80000
Thickness(um)	100-250	280-550
Soft bake min at 65°C	10-30	7-10
Soft bake min at 95°C	30-90	60-240
Post-exposure at 65°C	1	5
Post-exposure at 95°C	10-20	20-30
Development(min)	10-20	20-30

### 5.1.2 Fabrication of SU-8 microstructure

These wafers with inverted-trapezoid pit are used for fabricating SU-8 microstructure. Depending on the different number of rows of inverted-trapezoid pit, the second mask is designed as figure 5.2 shown. Three kinds of rows of inverted-trapezoid need to be filled with SU-8, so form different dimensions of SU-8 structure.

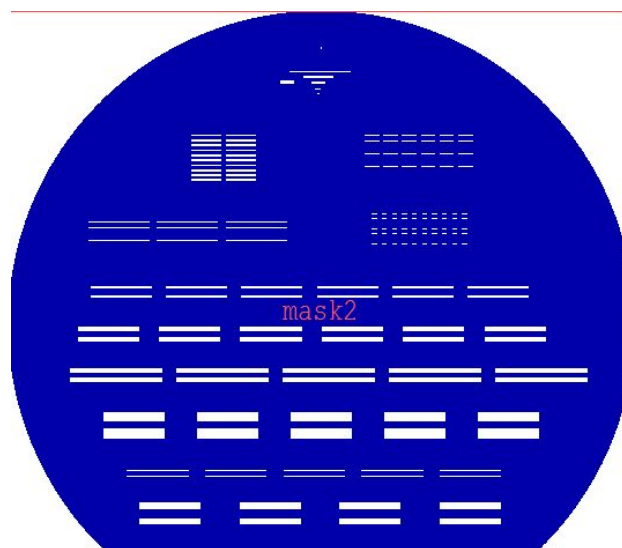


Fig. 5.2 mask for SU-8 microstructure

## Carbonization of SU-8 based electrode for MEMS supercapacitors

For depositing different thickness SU-8 films, wafer 4, wafer 5, and wafer 6 apply various photolithography process. Table 12 lists the process details.

Table .12 SU-8 process details

Process	Wafer 4	Wafer 5	Wafer 6
Wafer cleaning			
Dehydration			
Spin-coat	SU-8 2150 ①Spin speed 500 rpm for 10s ②Spin speed 1500 rpm for 30s	SU-8 2150 ①Spin speed 500 rpm for 10s ②Spin speed 2000 rpm for 35s	SU-8 100 ①Spin speed 1500 rpm for 40s
Soft bake	①65°C for 20mins ②95°C for 240mins	①65°C for 20mins ②95°C for 210mins	①65°C for 20mins ②95°C for 90mins
Cool down	20mins	20mins	10mins
Exposure	100s	90s	60s
Post bake	①65°C for 1mins ②95°C for 30mins	①65°C for 1mins ②95°C for 30mins	①65°C for 1mins ②95°C for 10mins
Development	15mins	15mins	10mins
thickness	550~560um	450~500um	220~270um

Based on SU-8 is a high viscous polymer, it is very difficult to fill the inverted-trapezoid pit after spin coating process, and bubble in the inverted-trapezoid pit is difficult to exhaust that is main problem to impede SU-8 flow into the pit, as shown in Figure 5.3. The inverted-trapezoid pit is the root of SU-8 structure to increase adhesion between SU-8 structure and substrate. Presence of the bubble make the root invalid, it will directly affect the result of carbonation experiments. Therefore, vacuum pump is recommended during the soft bake process, the purpose is to eliminate bubble. Figure 5.4 shows the vacuum device. In the period of soft bake, use vacuum pump repeatedly to make bubbles floating on the surface of SU-8 structure, then use a needle to break the bubble. This method is effective for removing bubbles

## Carbonization of SU-8 based electrode for MEMS supercapacitors

and will not damage the structure. But it also cause non-uniform thickness of SU-8 film, the result of SU-8 thickness shows in table 12.

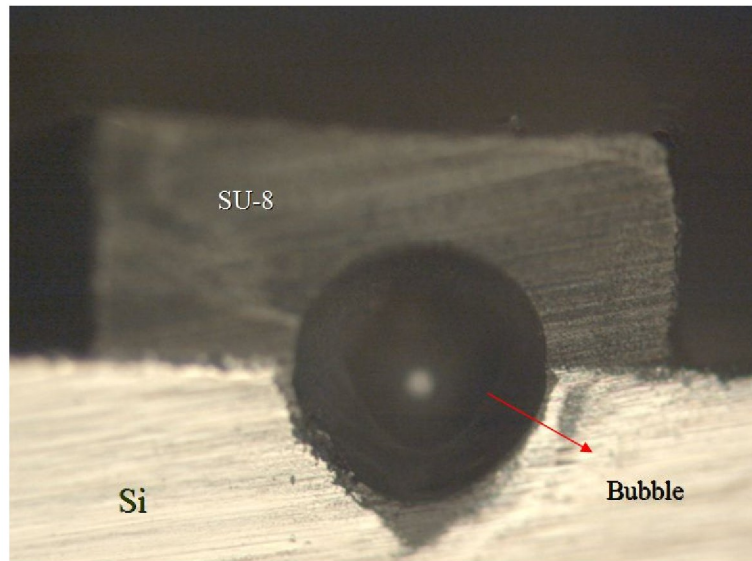


Fig. 5.3 Cross-section of SU-8 structure with bubble

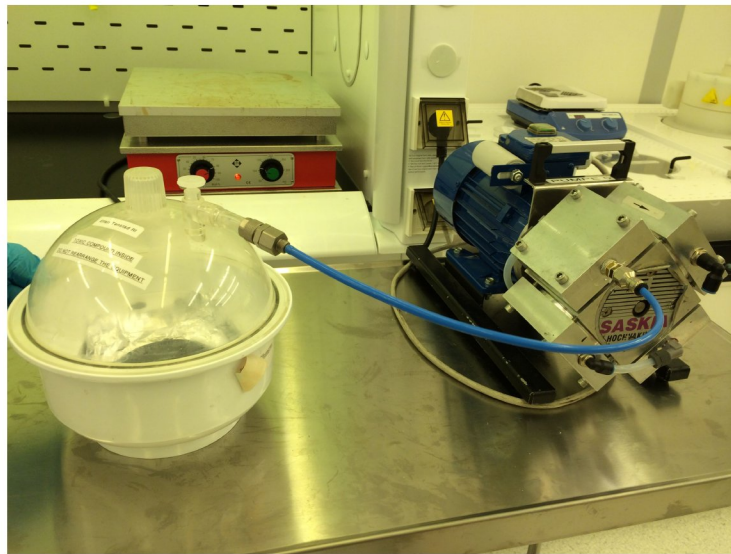


Fig. 5.4 vacuum pump

Figure 5.5 and figure 5.6 show the cross-section of SU-8 structure without bubble and the wafer after finishing SU-8 process, respectively. After fabricating SU-8 microstructure, these wafer should be cut into small pieces by Dicing saw for consecutive carbonization experiment.

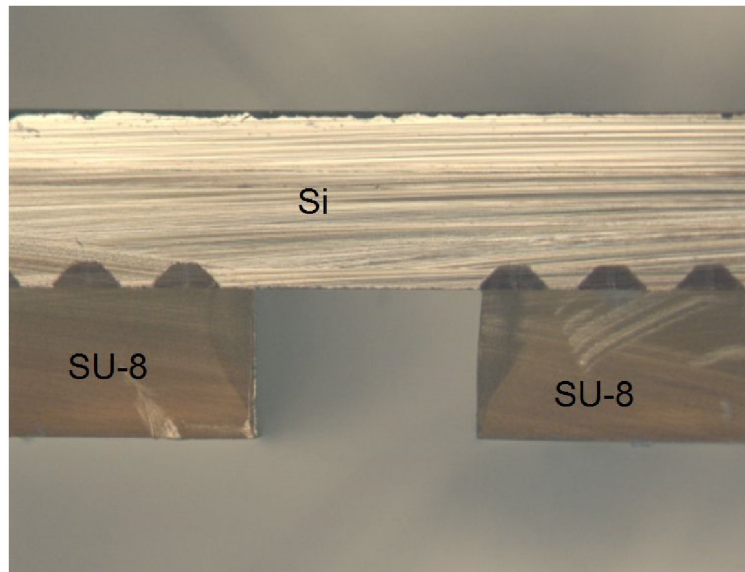


Fig. 5.5 cross-section of SU-8 structure



Fig. 5.6 wafer after finishing SU-8 process

## ***5.2 Carbonization process***

The purpose of carbonization process is to form activated carbon by the pyrolysis process of SU-8. The activated carbon are widely used as electrode material due to its porous structure that cause a large surface area. Activated carbon also has a relatively good electrical properties, and cheaper price. In this experiment, high temperature vacuum tube furnace GSL-1100 is used to supply an inert environment at the

## Carbonization of SU-8 based electrode for MEMS supercapacitors

temperature range of 600-1000 °C during carbonization process, as shown in figure 2.5. The inert gas is composed of 95% N<sub>2</sub> and 5% H<sub>2</sub>. The flow rate of gas is maintained at 1.5 Liter/minute throughout this carbonization process. Before this furnace works, the inert gas should be filled into the furnace for 1 hour to ensure absence of oxygen.

### 5.2.1 Carbonization process design

The carbon films fabricated were not always adherent to the substrate when finish pyrolysis process. There are three main reasons for this problem: 1.the adhesion between the substrate and SU-8 that depends on the roughness of the substrate. 2.gas evolution can affect adhesion during pyrolysis process, the good adhesion will be obtained if enough time is given for the gases to flow away. 3.the different coefficient of thermal expansion of the film and the substrate lead to thermal stresses in the film. For carbonization process, the adhesion is improved by controlling the heating and cooling rate, a slower heating and cooling rate allows more time for the gas evolution to escape. So the heating and cooling rate should be designed below 5 °C/minute.

In order to find out characteristics of SU-8 carbonization process, differential thermal analysis (DTA) is introduced. It can be seen in figure 5.7, which shows the downward spikes of curve for SU-8 runaway suddenly at about 450 °C, 700 °C, and 900 °C and then there are no more sharp downward spikes in the curve at higher temperatures. In other words, pyrolysis process of SU-8 occurs mainly at 450 °C, 700 °C, and 900 °C. These temperature is decomposition temperatures for SU-8, so holding a long time at these decomposition temperatures is necessary for full pyrolysis of SU-8. Holding time is shown in table 13.

Table. 13 Holding time for decomposition temperatures

Temperature(°C)	450	700	900	1000
Holding time (min)	60	90	60	60

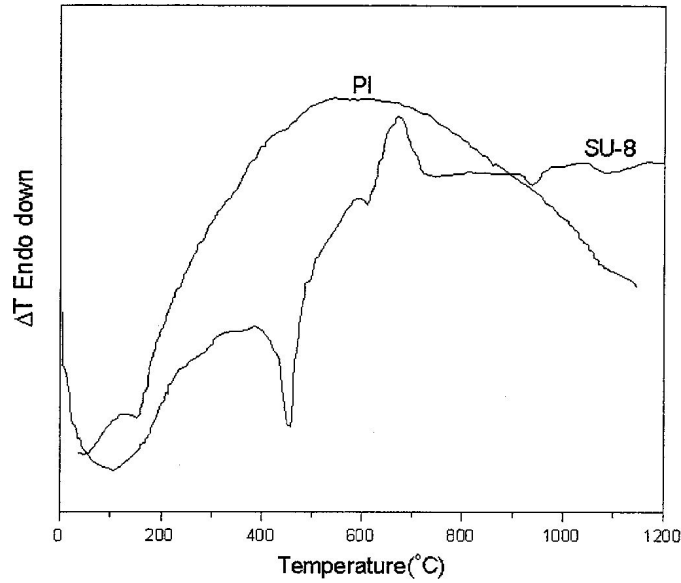


Fig.5.7 DTA of SU-8 and polyimide photoresists conducted in 5% H<sub>2</sub> and 95% N<sub>2</sub><sup>[41]</sup>

### 5.2.2 Temperature segment setting

The parameters of carbonization process are starting temperature, decomposition temperature, heating rate, holding time, and cooling rate. For fabricating activated carbon by pyrolyzing at temperatures in the range 600-1100°C is implemented in this experiment, so 700°C, 900°C and 1000°C are selected as the highest decomposition temperature, respectively. Thus thermal dynamic can be analyzed at different decomposition temperature.

Temperature segment setting for 700°C is shown in figure 5.8, and table 14 lists the detailed parameters. The heating/cooling rate is keeping below 5°C/minute.

Table. 14 carbonization process parameters for 700°C

Segment	Temperature(°C)	Time (mins)	Heating/cooling rate (°C/minute)
C01~C02	27~450	140	3.02
C02~C03	450~450	60	-----
C03~C04	450~700	110	2.27
C04~C05	700~700	90	-----
C05~C06	700~27	250	2.69

## Carbonization of SU-8 based electrode for MEMS supercapacitors

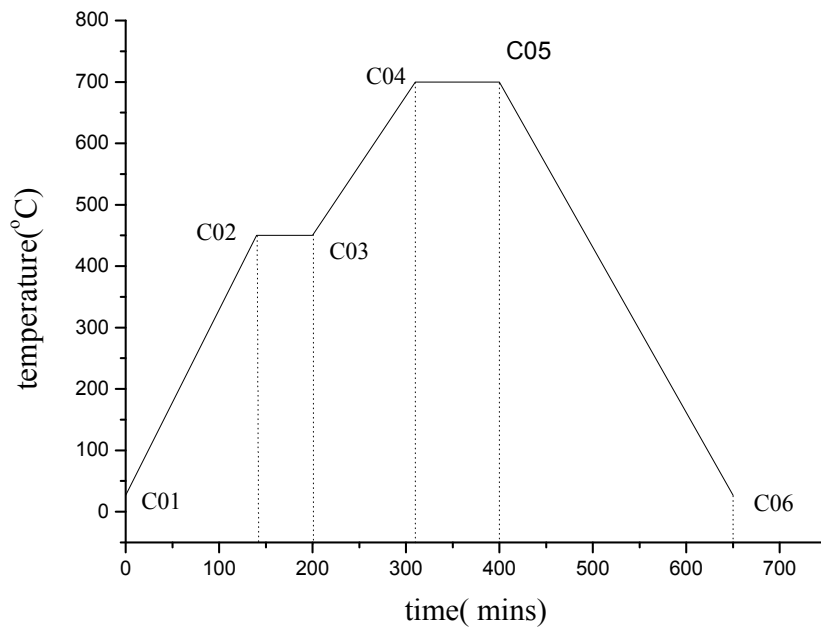


Fig. 5.8 Process with 5 segments, the highest decomposition temperature 700°C

For the highest decomposition temperature 900°C, temperature segment setting remains constant before 700°C. Then continue to heat to 900°C, table 15 lists the detailed parameters and figure 5.9 shows the Temperature control program.

Table. 15 carbonization process parameters for 900°C

Segment	Temperature(°C)	Time (mins)	Heating/cooling rate (°C/minute)
C01~C02	27~450	140	3.02
C02~C03	450~450	60	-----
C03~C04	450~700	110	2.27
C04~C05	700~700	90	-----
C05~C06	700~900	90	2.22
C06~C07	900~900	60	-----
C07~C08	900~27	350	2.49

## Carbonization of SU-8 based electrode for MEMS supercapacitors

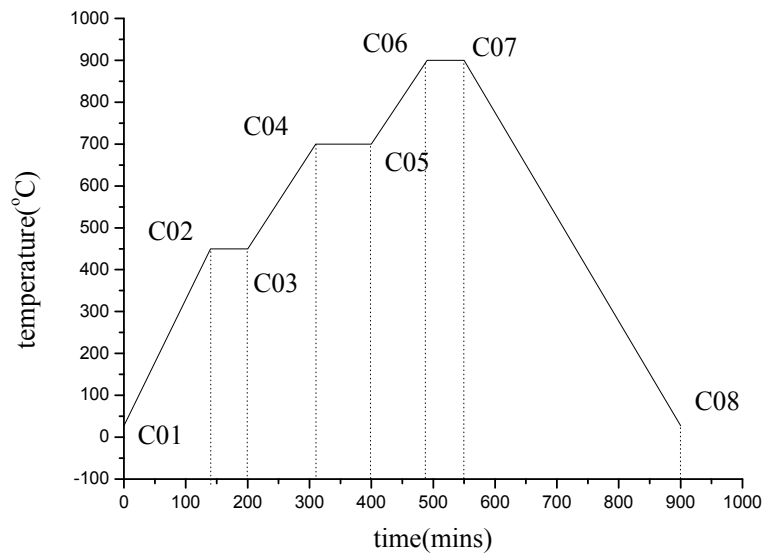


Fig. 5.9 Process with 7 segments, the highest decomposition temperature 900°C

Carbonization process for 1000°C has 9 segments temperature setting, as shown in figure 5.10. Along with the highest decomposition temperature rises, the time for cooling also should increase. Table 16 lists detailed parameters for this process.

Table. 16 carbonization process parameters for 1000°C

Segment	Temperature(°C)	Time (mins)	Heating/cooling rate (°C/minute)
C01~C02	27~450	140	3.02
C02~C03	450~450	60	-----
C03~C04	450~700	110	2.27
C04~C05	700~700	90	-----
C05~C06	700~900	90	2.22
C06~C07	900~900	60	-----
C07~C08	900~1000	40	2.5
C08~C09	1000~1000	60	-----
C09~C10	1000~27	390	2.49

## Carbonization of SU-8 based electrode for MEMS supercapacitors

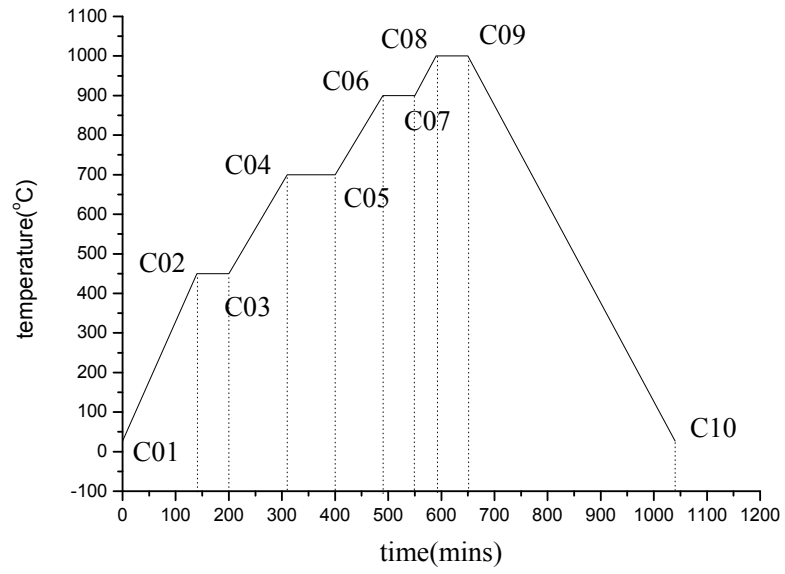


Fig. 5.10 Process with 9 segments, the highest decomposition temperature 1000°C

## Chapter 6 Characterization of Carbonization Process and Carbon Films

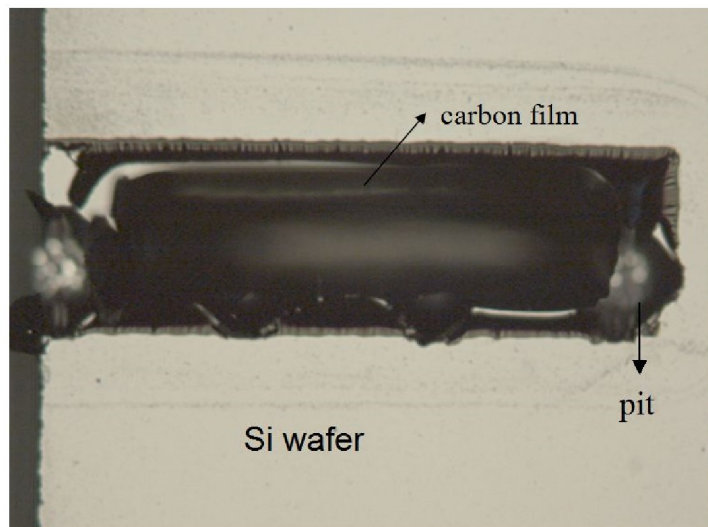
SU-8 structure film derived carbon film by carbonization process. In this chapter, the feature of carbon film is analyzed by Microscopy and SEM. SU-8 structure film that is before carbonization compare with the carbon film that is after carbonization, obtaining characterization of carbonization process.

### 6.1 *Film adhesion analysis*

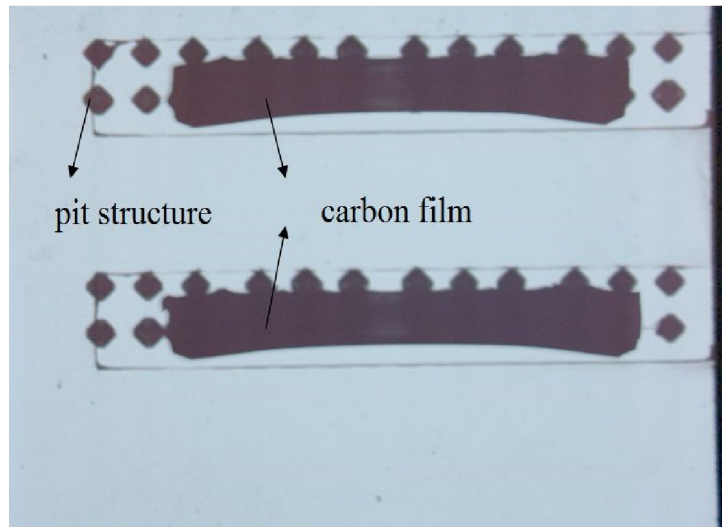
In chapter 5, the thickness of SU-8 for these three wafers are 550um, 500um, and 250um. So divide them into two groups for adhesion analysis, thick film and thin film structure.

#### 6.1.1 Thick film structure analysis

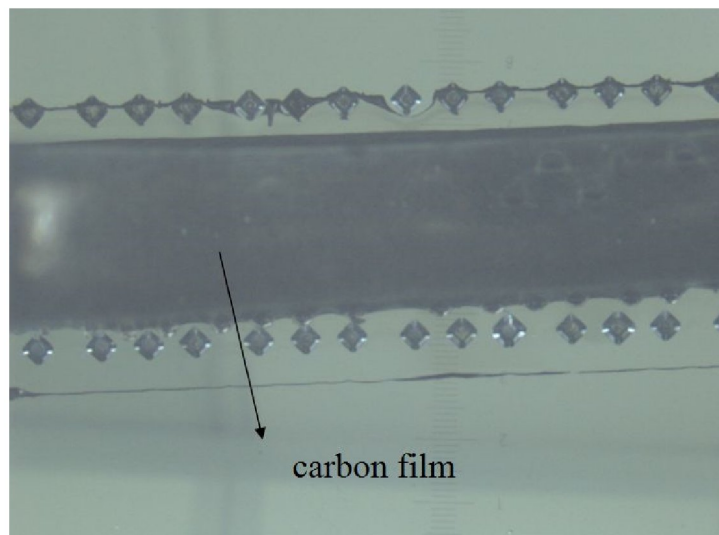
When the highest carbonization temperature is 700°C, the result of film adhesion is shown in figure 6.1 for thick SU-8film. Short structure with single row root shows in figure 6.1(a), carbon film is locked firmly on the substrate and structure has not been damaged during carbonization process.



(a) short structure with single row root



(b) long structure with 2 rows root



(c) long structure with 6 rows root

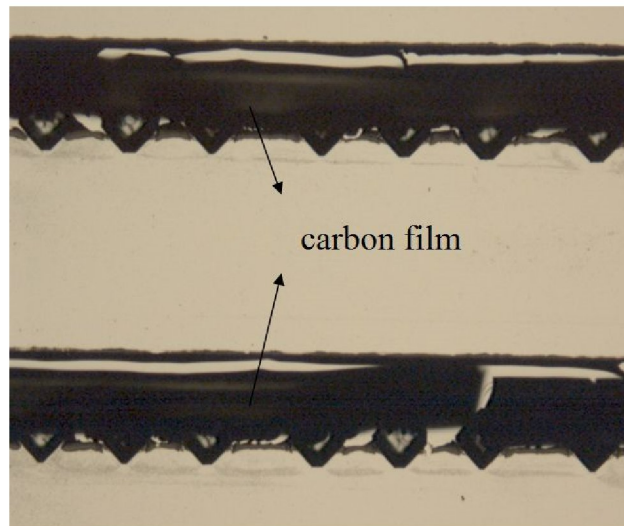
Fig. 6.1 Picture of thick SU-8 film derived carbon films at 700 °C

Long structure with 2 rows root also didn't peel off from the substrate, but both ends of the structure are warping and structure did not appear breakage. For long structure with 6 rows root (Fig. 6.1c), the phenomenon of warping also happens at ends of structure, unlike long structure with 2 rows that has a serious warping. There has two reasons for the warping phenomenon may be caused. The first is the concentration of stress that is from thermal stress due to expansion coefficient of SU-8 and silicon mismatch, and the tensile force is given by inverted-trapezoid pit that can impede the thermal stress. But the tensile force is not enough to prevent the thermal stress at ends of the thick structure, so as we have seen the warping

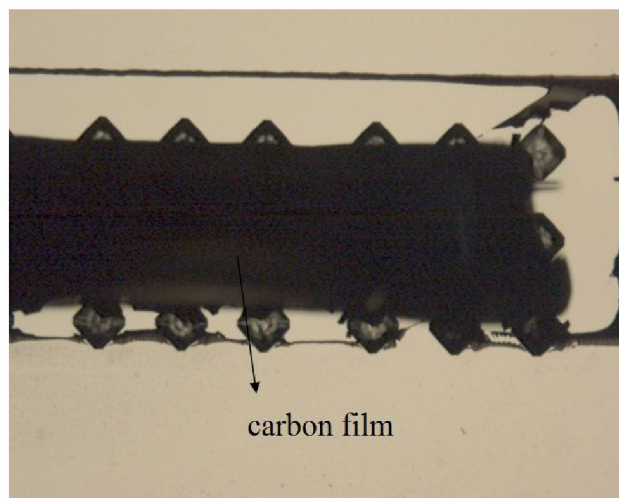
## Carbonization of SU-8 based electrode for MEMS supercapacitors

phenomenon. The second is shrinkage, that causes the structure break away the bound of inverted-trapezoid pit after carbonization process, so thermal stress bring the warping at ends of structure.

Figure 6.2 shows picture of thick SU-8 film derived carbon films at highest carbonization temperature 900°C. Long structure with single row root is still adherent on the substrate, and the warping phenomenon still exist. Because of non-uniform thickness in some structure, as figure 6.2(a) shows the rupture in the structure. Long structure with 3 rows root locked firmly on the substrate without warping phenomenon, and structure is undamaged.



(a) long structure with single row root

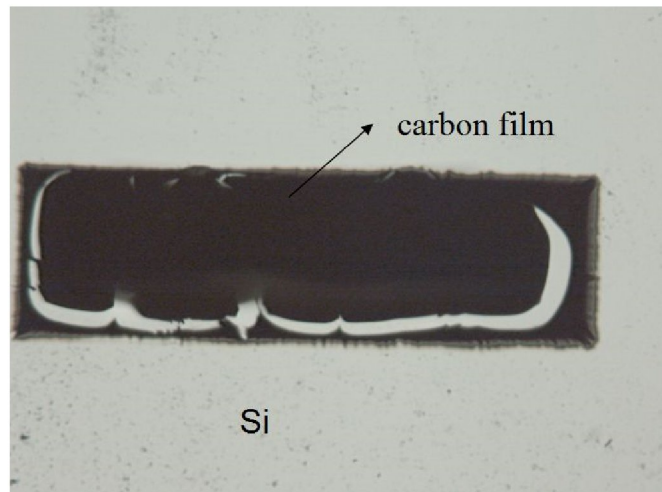


(b) long structure with 3 rows root

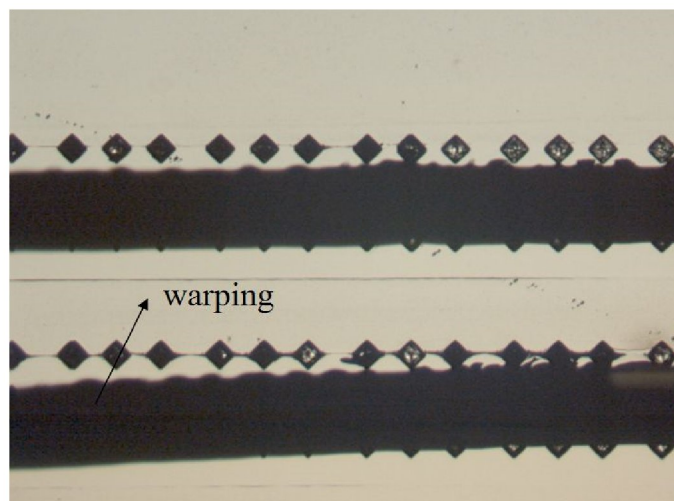
Fig.6.2 Picture of thick SU-8 film derived carbon films at 900°C

## Carbonization of SU-8 based electrode for MEMS supercapacitors

Compared with the results of the above, when the highest carbonization temperature is 1000°C, as shown in figure 6.3. Short structure with single row root has perfect adhesion with the substrate. Contrast with figure 6.2(b), Long structure with 3 rows root although doesn't peel off, but there has very serious warping phenomenon. That is because thermal stress is more obvious at 1000°C than at other temperatures, the structure gets rid of the inverted-trapezoid pit during carbonization process, additionally greater shrinkage is also the reason for this problem. For small size SU-8 structure, the deformation of structure is not enough to break away the bond of root after carbonization process, therefore, perfect adhesion is obtained at the whole temperatures.



(a) short structure with single row root



(b) long structure with 3 rows root

Fig. 6.3 Picture of thick SU-8 film derived carbon films at 1000°C

### 6.1.2 Thin film structure analysis

The thickness of SU-8 film is 220um~270um for thin film structure. Figure 6.4 shows picture of thin SU-8 film derived carbon films at highest carbonization temperature 700°C. Every structure doesn't peel off from the substrate, and warping phenomenon disappeared.

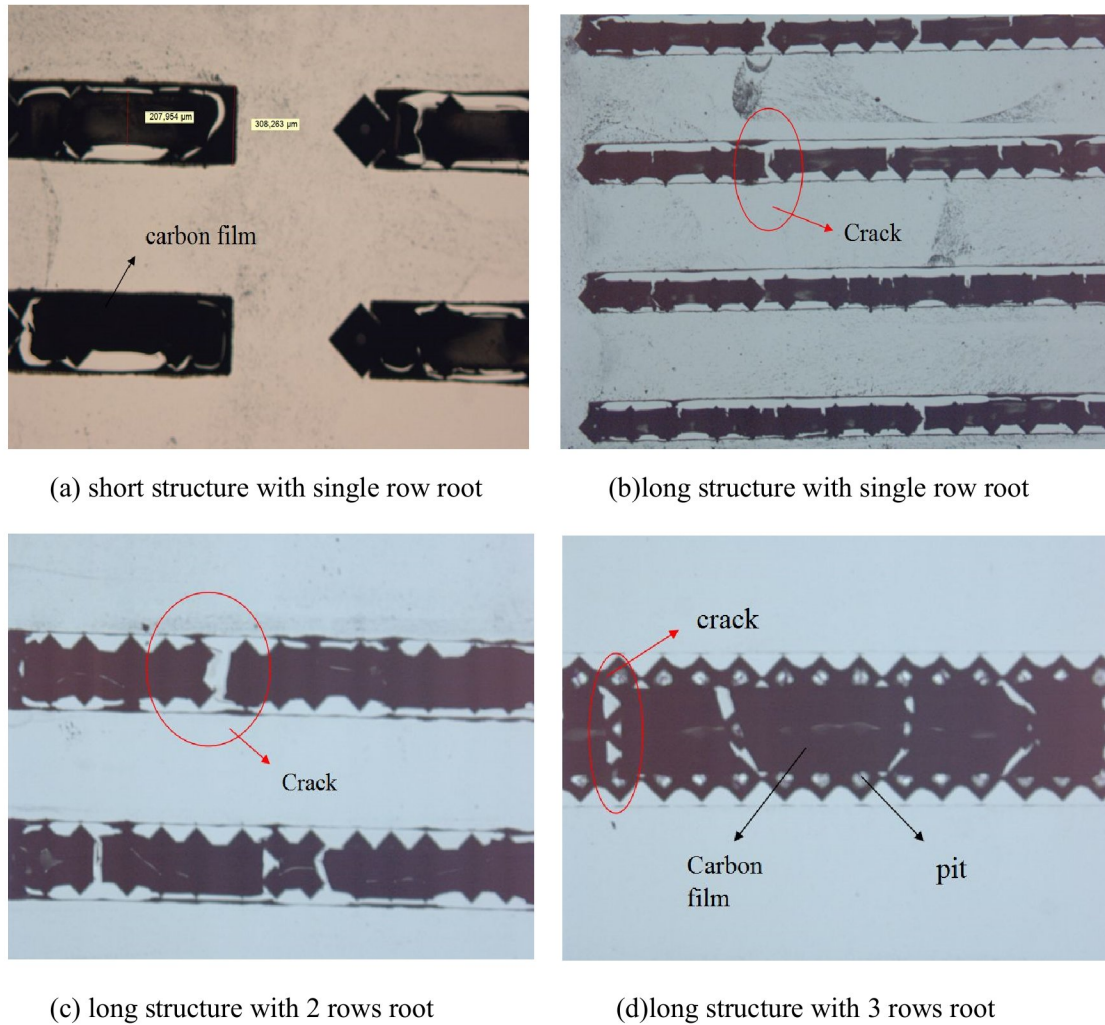
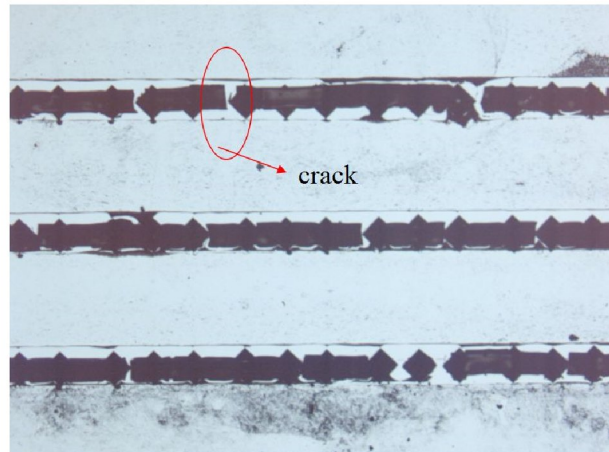


Fig. 6.4 Picture of thin SU-8 film derived carbon films at 700°C

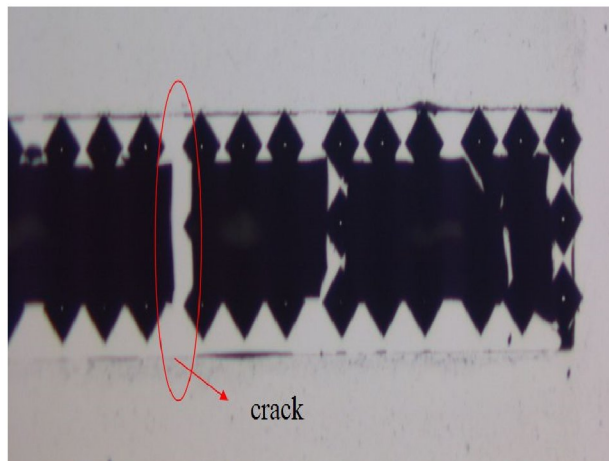
The result of short structure with single row root is still excellent, but in other structure a new problem has arisen that is crack, as shown in figure 6.4 (b), (c) and (d). Since the existence of thermal stress during carbonization process, the deformation occurs in the material, and the structure can not get rid of the shackles of inverted-trapezoid pits. Additionally, the thin film can not endure the interaction of these forces, so the thin film is prone to breakage after the carbonization process.

## Carbonization of SU-8 based electrode for MEMS supercapacitors

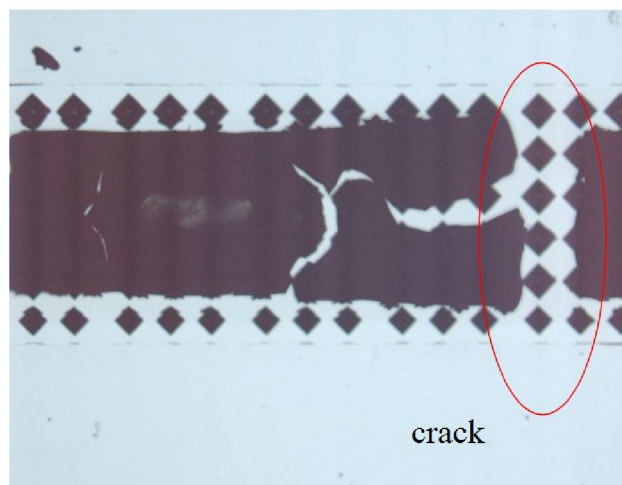
For highest carbonization temperature is  $900^{\circ}\text{C}$ , the result is shown in figure 6.5. All of the structures are locked firmly on the substrate by inverted-trapezoid pit. The same problem of crack appears in long film structure.



(a) long structure with single row root



(b) long structure with 3 rows root

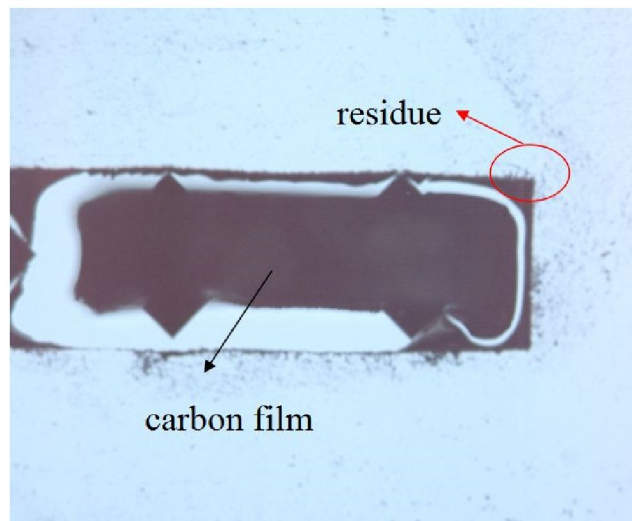


(c) long structure with 6 rows root

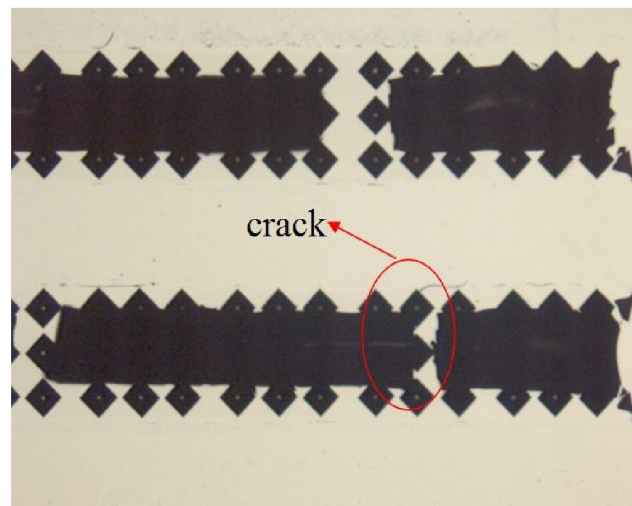
Figure. 6.5 Picture of thin SU-8 films derived carbon films at  $900^{\circ}\text{C}$

## Carbonization of SU-8 based electrode for MEMS supercapacitors

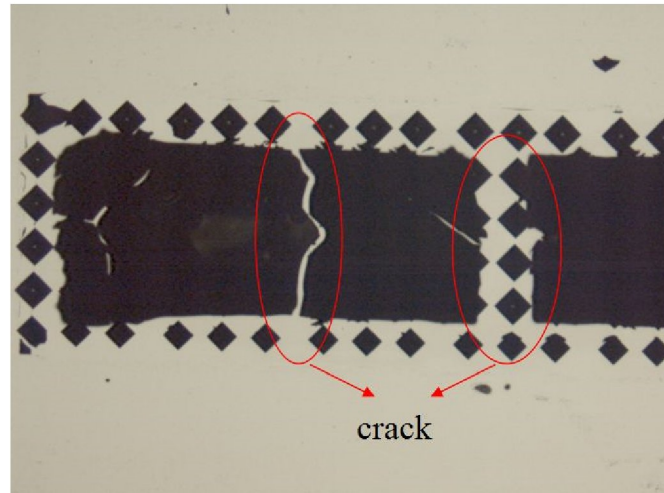
As shown in figure 6.6, when the highest carbonization temperature is 1000°C, the carbon film structure doesn't peel off from the substrate. The short structure with single row root has no crack in the structure, and for long structure with 3 rows root and long structure with 6 rows root exist prevalent crack phenomena after carbonization process. The residue of carbon film can be found on the edge of structure in every picture, and it is inevitable during this process, because of SU-8 is a high viscous polymer.



(a) short structure with single row root



(b) long structure with 3 rows root

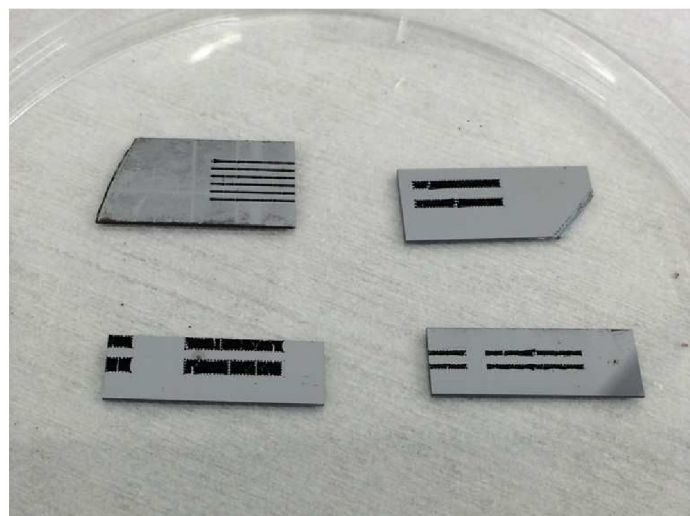


(c) long structure with 6 rows root

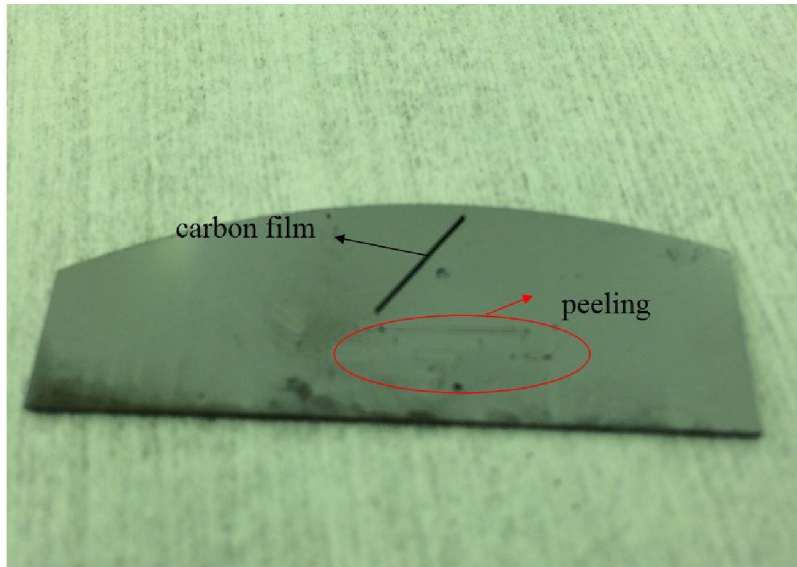
Fig. 6.6 Picture of thin SU-8 film derived carbon films at 1000°C

### 6.1.3 Summary

The function of inverted-trapezoid pit as the root is obvious for SU-8 film structure during the carbonization process, figure 6.6 shows comparison results between with inverted-trapezoid pit and without any pit. As shown in figure 6.6(a), the structure doesn't peel off from the substrate, and the all structure without any pit peel off the substrate after carbonization process. So the inverted-trapezoid pit as root for structure can improve the adhesion between C-MEMS and substrate.



(a) carbon film with inverted-trapezoid pit



(b)carbon film without inverted-trapezoid pit peel off

Fig. 6.6 Contrast of carbon film with inverted-trapezoid pit and carbon film without inverted-trapezoid pit

From the above analysis, the thin film structure with this inverted-trapezoid pit can prevent the warping phenomenon, but crack phenomenon is widespread, the result is adverse for the thick film. Under the condition that keep the dimension of inverted-trapezoid pit unchanging, the less row root and smaller SU-8structure can avoid these problem, and try to keep the pit under the middle of the structure. Furthermore, the dimensions of inverted-trapezoid pit need modify for different size SU-8structure, finally obtain the parameters of excellent matching.

### **6.2 Weight loss analysis**

Based on the differential thermal analysis (DTA) curve in figure5.7, the temperature of several peaks and valleys are chosen for weight loss analysis. The pyrolysis process of SU-8 may occur at these temperature, and the pyrolysis process means the weight of the SU-8 film will reduce during this process. So these temperatures are 350°C, 450°C, 550°C, 700°C, 900°C and 1000°C, respectively. By measuring the weight of SU-8 structure before and after carbonization process,

## Carbonization of SU-8 based electrode for MEMS supercapacitors

calculate the weight loss. Table 17 lists the weight of SU-8 at these temperatures before and after carbonization process.

Table. 17 Contrast of SU-8 weight before and after carbonization process

W \ T	350°C	450°C	550°C	700°C	900°C	1000°C
before	①0.0732g	①0.0739g	①0.0648g	①0.0724g	①0.1404g	①0.0749g
carbonization	②0.0509g	②0.0354g	②0.0356g	②0.0695g	②0.0319g	②0.0452g
after	①0.0695g	①0.0576g	①0.0253g	①0.0209g	①0.0351g	①0.0149g
carbonization	②0.0489g	②0.0275g	②0.0142g	②0.0198g	②0.0079g	②0.0091g
Weight%	96%	78%	39%	29%	25%	20%

From 350°C to 700°C, the weight of SU-8 has a significant reduction with increasing temperature. The weight loss is tardy during the temperature from 700°C rising to 1000°C, and weight loss almost stops at 1000°C. Figure 6.7 is thermogravimetric analysis of SU-8 derived carbon films that plotted based on table 17.

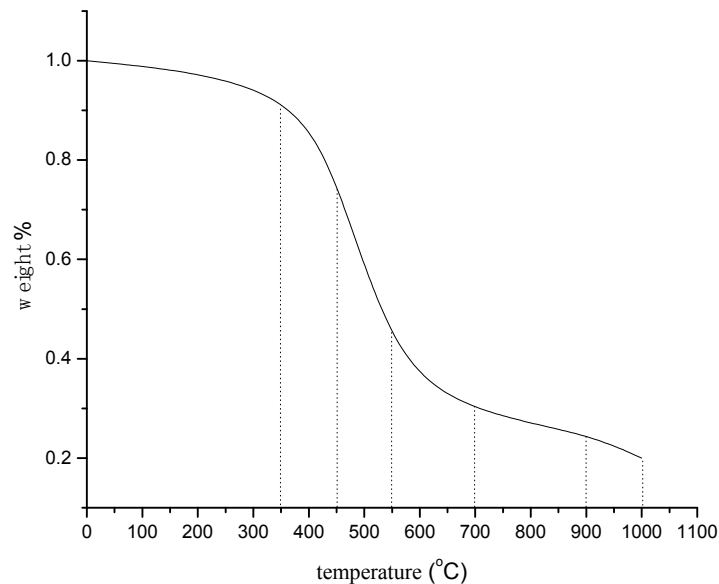


Fig.6.7 Thermogravimetric analysis of SU-8 derived carbon films

### 6.3 Microscopy analysis

#### 6.3.1 SEM images analysis

The surface morphology of carbon film that fabricated in carbonization process is analyzed by scanning electron microscope(SEM), figure 6.8 shows the SEM pictures with different carbonization temperatures, magnification is 6890x. As can be seen from the high resolution images, the carbon structure is pore free when the the highest temperature are 700°C and 900°C, and a few pore can be found in the carbon film when the the highest temperature is 1000°C.

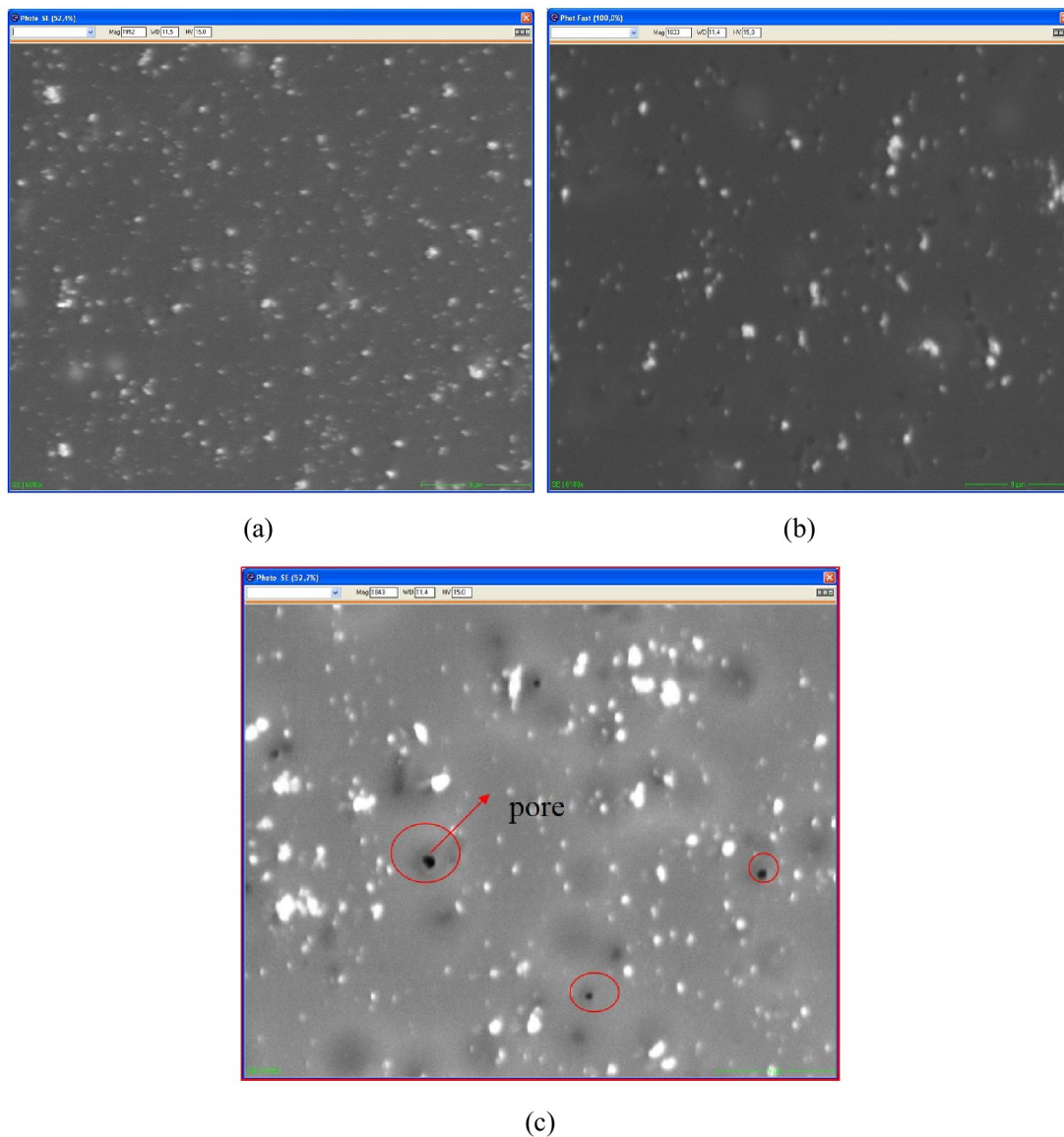


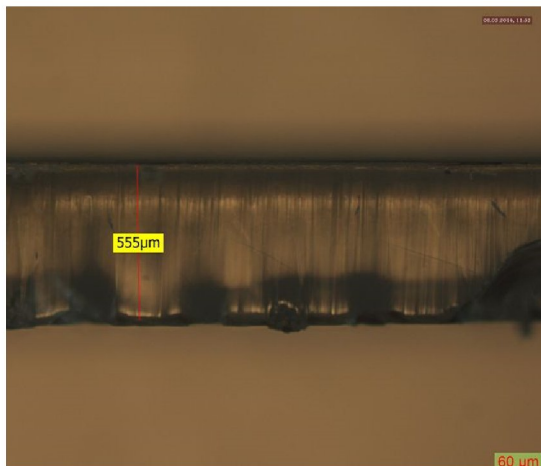
Fig. 6.8 SEM image of SU-8 derived carbon films, (a) at 700°C, (b) at 900°C, (c) at 1000°C.

### 6.3.2 Vertical shrinkage

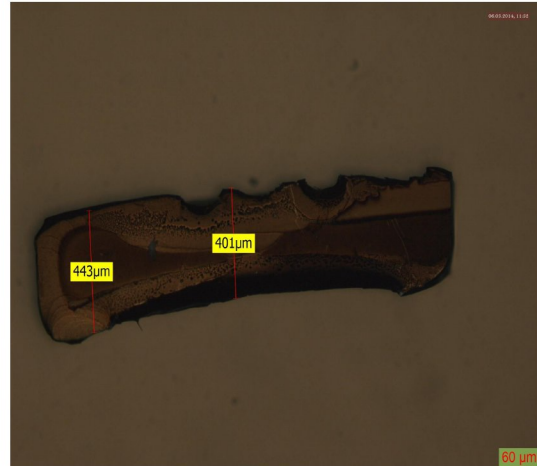
The thickness of the structure is measured by Microscope I Leica DM4000M after carbonization process. The detailed comparison of the data is listed in table 18. the thickness of carbon film will decrease with the temperature increasing. Figure 6.9 shows the change of thickness for the same SU-8 structure.

Table. 18 Vertical shrinkage for SU-8 derived carbon films

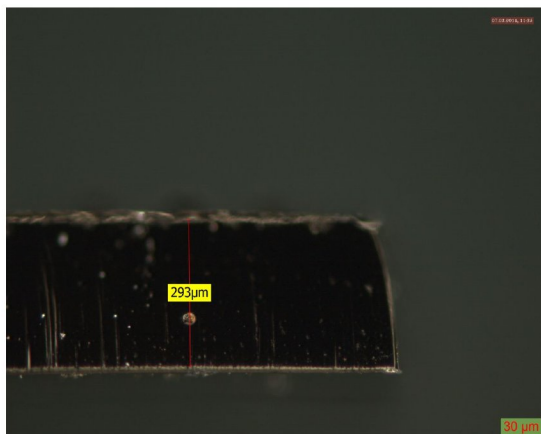
Temperature of pyrolysis(°C)	Thickness of SU-8 film(um)	Thickness of carbon film(um)	% Reduction
700	555	401	27.7%
900	555	293	47.2%
1000	555	222	60%



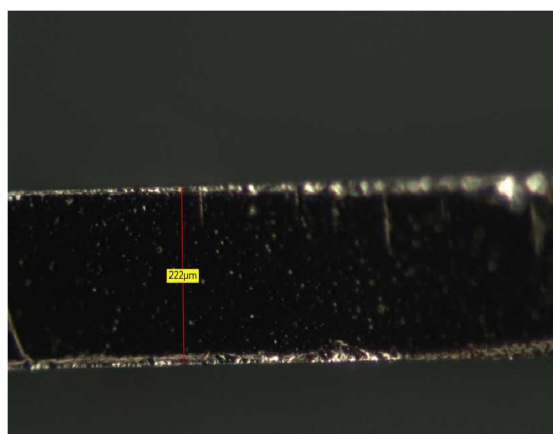
(a) Thickness before carbonization process



(b) Thickness after carbonization process at 700°C



(c) Thickness of carbon film at 900°C



(d) Thickness of carbon film at 1000°C

Fig. 6.9 Thickness of SU-8 derived carbon films at different pyrolysis temperatures

## **Carbonization of SU-8 based electrode for MEMS supercapacitors**

The warping phenomenon and crack phenomenon cause the uneven thickness distribution of carbon film after carbonization, that has been analyzed in chapter 6.1. And the thickness of ends of structure is thicker than the middle of structure. As shown in figure 6.9(b), there are two different thickness for this structure, the thickness of the middle of the structure that located near the inverted-trapezoid pit is selected for vertical shrinkage analysis.

## **Chapter 7 Conclusion**

As a result of my experiments in this project, the inverted-trapezoid pits successfully prevent the structure film from peeling off from the substrate. For fabricating the inverted-trapezoid pits on a silicon wafer, the alignment of the open window in the masks become extremely important for the final shape and structure of the pits. We have to note that there has an angle of  $45^\circ$  between  $\langle 110 \rangle$  surface and  $\langle 100 \rangle$  surface, the  $\langle 110 \rangle$  surface appearing in a right alignment is the key for successfully fabricating the inverted-trapezoid pits. The depth of inverted-trapezoid structure depends on the RIE etching. In order to obtain a deeper RIE anisotropic etching pit, the etching parameters, such as the ratio of  $\text{SF}_6$  and  $\text{O}_2$ , system pressure as well as RF power, have to be optimized by a large number of the development experiments.

SU-8 as a high viscous polymer, in the spin coating a vacuum pump is introduced for eliminating bubbles and prompting SU-8 to flow into the inverted-trapezoid pits during the soft bake step. The fabricated SU-8 films are carbonized in an inert atmosphere at different temperatures such as  $700^\circ\text{C}$ ,  $900^\circ\text{C}$  and  $1000^\circ\text{C}$ . Our developed processes are able to fabricate carbonized SU-8 films which firmly stand on the substrate. However, we find that the warping phenomenon appears in the thick film and cracks occur in the thin film structures. The design of different size of SU-8 structures depends on the dimension of the inverted-trapezoid pits to ensure that the inverted-trapezoid pits are always covered by the SU-8 structure after the carbonization. Finally, weight loss and vertical shrinking of the SU-8 at the different carbonation temperatures are characterized.

## Reference

- [1] Martin Winter, Ralph J. Brodd, What are batteries, fuel cells, and supercapacitors, 2004.
- [2] <http://zh.scribd.com/doc/6985249/Introduction-to-Super-Capacitors>.
- [3] <http://www.chemi-con.co.jp/e/company/pdf/20100330-1>.
- [4] Bus project, Vinzenz V. Haervi, Drago Martinovic, An advance energy stroage specification based on experiences with the TOHYCO-Rider, Industrial Electronics Society, 2007.
- [5] <https://www.google.no/search?hl=zh-CN&q=classification%20of%20supercapacitors&um=1&ie=UTF-8>.
- [6] Mustafa Sami Ata, B. SC, Advanced Materials and Fabrication Methods for Electrochemical Supercapacitors, 2012: 10-14.
- [7] Alar Janes, Heisi Kurig, Enn Lust, Characterisation of activated nanoporous carbon for supercapacitor electrode materials, Carbon 45 (2007) 1226–1233.
- [8] Mustafa Sami Ata, B. SC, Advanced Materials and Fabrication Methods for Electrochemical Supercapacitors, 2012: 15-22.
- [9] <http://en.wikipedia.org/wiki/Supercapacitor>.
- [10] Wei Sun, PhD Thesis, 2011.
- [11] John R. Miller, Patrice Simon, Fundamentals of electrochemical capacitor design and operation, 2008.
- [12] R.A. Rightmire, Electrical energy storage apparatus, U.S., Patent 3 288 641, 1970.
- [13] X. Andrieu, Ultracapacitors for portable electronics. Energy Storage Systems for Electronics: New Trends in Electrochemical Technology. 1. 2000. p. 521.
- [14] S. Hadzi-Jordanov, et al., Reversibility and Growth Behavior of Surface Oxide Films at Ruthenium Electrodes. Journal of The Electrochemical Society, 1978. 125(9): p. 1471-1480.
- [15] <https://www.google.no/search?um=1&hl=zh-CN&tbn=isch&sa=1&q=maxwell+boostcap&oq=Maxwell>.
- [16] A brief history of supercapacitors, 2010.
- [17] Beidaghi M. and C. Wang, Micro-super capacitors based on three dimensional interdigital polypyrrole/C-MEMS electrodes. Electrochemical Acta 56(25): 9508-9514.

## **Carbonization of SU-8 based electrode for MEMS supercapacitors**

---

- [18] Durou, H, D. Pech, et al. Wafer-level fabrication process for fully encapsulated Micro-supercapacitors with high specific energy. *Micro system Technologies* 18(4): 467-473.
- [19] In, H. J., S. Kumar, et al. Nanostructured Origami 3D fabrication and assembly of electrochemical energy storage devices. *Nanotechnology*, 2005.
- [20] Penmatsa, V., H. Kawarada, et al. Fabrication of carbon nanostructures using photo-nanoimprint lithography and pyrolysis, 2012.
- [21] Yingge Wang, CARBONIZATION of SU-8 for THREE DIMENSIONAL MEMS SUPERCAPACITORS, 2012.
- [22] P.Sharma, et al., A review on electrochemical doublelayer capacitors, *Energy Convers Manage*, pp. 2901–2912, December 2010.
- [23] Y. Q. Jiang, Q. Zhou, L. Lin, *Micro Electro Mechanical Systems*, 2009. MEMS 2009. IEEE 22nd International Conference on, 25-29 Jan. 2009, Sorrento, Italy.
- [24] Jong-Huy Kim, Ashok K. Sharma, Yong-Sung Lee, Synthesis of polypyrrole and carbon nano-fiber composite for the electrode of electrochemical capacitors, *Materials Letters* 60 (2006) 1697–1701.
- [25] E. Frackowiak, V. Khomenko, K. Jurewicz, et al., Supercapacitors based on conducting polymers/nanotubes composites, *Journal of Power Sources* 153(2006) 413–418, Short communication.
- [26] Joo-Hwan Sung, Se-Joon Kim, Kun-Hong Lee, Fabrication of all-solid-state electrochemical microcapacitors, *Journal of Power Sources* 133 (2004) 312–319.
- [27] Joo-Hwan Sung, Se-Joon Kim, Flexible micro-supercapacitors, Short communication, *Journal of Power Sources* 162 (2006) 1467–1470.
- [28] H. Manhee et al., 3D microfabrication with inclined/rotated UV lithography, *Sensors and Actuators :A*, vol.111, pp. 14–20, March 2004.
- [29] Avinash P. Nayak et al, *Wet and Dry Etching*, University of California .
- [30] Jie Gong, Zirong Tang, Tielin Shi, Guanglan Liao and Shiyuan Liu, Improved Adhesion Between C-MEMS and Substrate by Micromechanical Interlocking, January 5-8, 2009.
- [31] K. Sato et al. Characterization of orientation-dependent etching properties of single-crystal silicon: effects of KOH concentration (*Sensors and Actuators A* 64 (1988) 87-93).
- [32] M. Shikida, K. Sato, K. Tokoro, D. Uchikawa, Dept of Micro Systems Engineering, Nagoya University, Japan.

## **Carbonization of SU-8 based electrode for MEMS supercapacitors**

- [34] Wet-Chemical Etching of Silicon, 2013.
- [35] Jansen HV, Deboer MJ, Legtenberg R, Elwenspoek MC (1995) The black silicon method: A universal method for determining the parameter setting of a fluorine based reactive ion etcher in deep silicon trench etching with profile control, pp.115-120.
- [36] [http://en.wikipedia.org/wiki/SU-8\\_photoresist](http://en.wikipedia.org/wiki/SU-8_photoresist).
- [37] Teh W H et al 2005 Effect of low numerical-aperture femtosecond two-photon absorption on (SU-8) resist for ultrahigh-aspect-ratio microstereolithography J. Appl.
- [38] A del Campo and C Greiner, SU-8: a photoresist for high-aspect-ratio and 3D submicron lithography, May 2007.
- [39] [http://www.microchem.com/products/su\\_eight.htm](http://www.microchem.com/products/su_eight.htm).
- [40] Permanent Epoxy Negative Photoresist PROCESSING GUIDELINES FOR:SU-8 2100 and SU-8 2150, Micro Chem.
- [41] S. Amit, Pyrolysis of negative photoresists to fabricate carbon structures for microelectromechanical systems and electrochemical applications, Journal of The Electrochemical Society, vol.149, pp. 78-83, January 2002.
- [42] Rob Legtenberg, Henri Jansen, Meint de Boer, and Miko Elwenspoek, Anisotropic Reactive Ion Etching of Silicon Using SF<sub>6</sub>/O<sub>2</sub>/CHF<sub>3</sub> Gas Mixtures, The Electrochemical Society, pp. 2021-2028, June 1995.

## **Acknowledgement**

At first, I would like to thank my supervisor, Professor Xuyuan Chen. His great support and advice help me to finish this project.

I also grateful to the IMST lab engineers, Ms. Zekija.Ramic, Mr. Thomas.Hoff, and Mr. Ragnar.N.Berg for their generous help in my cleanroom experiments.